The Pennsylvania State University
The Graduate School

FEW-BODY PROPERTIES OF INTERACTING SPINS IN III-V SEMICONDUCTORS

A Dissertation in
Physics
by
Ryan Woodworth

Submitted in Partial Fulfillment
of the Requirements
for the Degree of

Doctor of Philosophy

August 2009

The dissertation of Ryan Woodworth was reviewed and approved* by the following:

Gerald D. Mahan
Distinguished Professor of Physics
Dissertation Advisor, Chair of Committee

Nitin Samarth
Professor of Physics

Vincent H. Crespi
Professor of Physics
Professor of Materials Science and Engineering

Venkatraman Gopalan
Professor of Materials Science and Engineering
Associate Director, Center for Optical Technologies

Jayanth R. Banavar
Distinguished Professor of Physics
Head of the Department of Physics

*Signatures are on file in the Graduate School.

Abstract

We perform theoretical analyses of several novel device applications which make use of the distinctive electronic and optical properties of III-V semiconductors.

Electron spins in semiconductor quantum dots are a promising candidate for the physical realization of a solid-state quantum computer. Whenever three or more spins interact simultaneously, the system's full Hamiltonian is found to include nonlinear interactions that significantly influence its dynamics in experimentally relevant parameter regimes. We consider the implications of these results for the proposed implementations of known quantum algorithms; in particular, we describe a method for circumventing the four-body effects in an encoded system (four spins per logical bit) by the appropriate tuning of material parameters.

We calculate the spin coherence lifetime of a conduction electron in a semiconductor due to exchange scattering from neutral donors. The average lifetime is computed in two and in three dimensions using the Born approximation. We find that, for realistic values of the impurity concentrations, these lifetimes are comparable to those of spin decoherence mechanisms commonly ascribed to experimentally observed lifetimes.

We also develop a numerical model for charge diffusion in a GaAs heterostructure laser. We construct and solve rate equations for conduction electrons coupled to a single optical cavity mode in a microdisk. Our results extend previous theoretical approaches to diffusion and are consistent with applicable experiments.

Table of Contents

List of Figures

Acknowledgments

This document owes its existence principally to Dr. Gerald Mahan, my advisor. Not only is his knowledge of theoretical physics just as broad and refined in person as in his textbook, he is a master at cutting a problem into digestible pieces and then deciding which ones correspond to gaps in the published literature. I never left a meeting without feeling as though I were smart enough to have a doctorate.

I must also acknowledge the influence of Dr. Ari Mizel, my former advisor. His professional voice is the yin counterpart to Jerry's, insisting on common sense, awareness of mathematical rigor, and clear writing. Those things will benefit my career even if it is unrelated to my academic study.

Dr. Nitin Samarth and Dr. Rusko Ruskov expended considerable effort to educate me about microdisk fabrication and electron spin kinematics, even after it became obvious that my calculations would not aid their own research. And although our communication was limited, Dr. Daniel Lidar did his best to initiate me into the mysteries of quantum information processing.

I am indebted to the department's Graduate Recruiting Committee of 2000-2001 (Dr. Stephane Coutu, chair) for rolling the dice on what must have seemed a deliberately nonstandard application and CV. Dr. Vincent Crespi and Dr. Venkatraman Gopalan are the members of my thesis committee not named above; they always accommodated my circuitous logistical requests and always had informed questions ready when they arrived. Dr. Gary Gray and Dr. Francesco Costanzo, who I have never met nor spoken to, nevertheless saved me weeks of coding with their LaTeX dissertation template (http://www.esm.psu.edu/psuthesis/).

Beside every successful graduate student walks a small crowd of people who help to maintain his or her mental health. In this regard I could easily spend another page each on Sara Kimbell, Christine Kraemer, Jess Meeker, Elizabeth Nickrenz, Melissa Ortz, Chris Peters, Jessica Roy, Alastair Thompson, George Vines, Amanda Weimer, and Matt Wyzykowski. Without them, this research would not have been possible.

Chapter 1

Introduction

Beginning with the first solid-state transistors in the 1940s, semiconductors have become as ubiquitous as electronics technology itself. Most semiconductor applications originally employed silicon, still widely used, because it is easily machined and its properties are widely tunable using dopants. Newer photonic devices, on the other hand, rely increasingly on diatomic crystals such as III-V and II-VI (named for the corresponding columns in the periodic table), whose huge band gaps encourage long electron-hole pair lifetimes, and whose electro-optical properties can often be adjusted simply by injecting current. III-V materials are preferred to silicon in heterostructure systems, for example, because alloying alters their lattice constants only slightly. They are also particularly suited to novel spintronic applications, because the two atomic diameters are sufficiently different to create a high spin-orbit coupling while still possessing a large band gap. [1, 2, 3, 4]

1.1 Few-body spin operators in quantum computing

The underlying theory of quantum computation can be summarized in one sentence: "Instead of a conventional bit of information, which is either ON or OFF, allow the bit to be a two-state quantum system (qubit), therefore a superposition of ON and OFF with a relative phase." This leads eventually to a comprehensive reformulation of Boolean algebra which will not be summarized here (see Ref. [5] for a thorough quantitative discussion). As in the classical case, however, algorithms are implemented using logic gates, each joining two or more qubits temporarily.

Chapter 2 of this dissertation analyzes a set of qubits represented by a Hamiltonian of

coupled spin-1/2 particles. Previous research had shown [6] that when three or more qubits interact simultaneously, the energies of the resulting quantum states can vary nonlinearly as compared to a superposition of pairwise couplings only. We generalize those results and propose a method for avoiding the nonlinear effects by delocalizing each bit of information across a set of four spins. It should be emphasized that this line of reasoning does not undermine previously published quantum algorithms which assume Heisenberg exchange interactions, but merely suggests that the choice of algorithm be influenced by the types of qubit-qubit couplings readily available in a given apparatus. (The situation is analogous to that of classical computing before the advent of compiled languages: each piece of software had to be rewritten from scratch whenever memory or processor configurations changed [7].)

The experimental situation is characterized by some dozen or sixteen classes of engineering proposals, each with its own advantages and drawbacks [8, 9]. For example, a qubit might be realized as two proximate energy levels of a mercury ion in a laser trap, or the direction of a localized current in a superconductor, or the average magnetization of nuclear spins in a macroscopic cell of fluid [5]. A system is considered a good candidate when each computational unit can be confined to two possible energy states for long periods of time, and is relatively easy to shield from thermal fluctuations and other dissipative mechanisms (most quantum algorithms are extremely sensitive to noise). Given the versatility of III-V semiconductors, it was perhaps inevitable that one proposal would involve a precisely fabricated GaAs microstructure in which two-state systems can be isolated [10]. We do not claim to have settled this issue by basing our calculation on a model system of GaAs quantum dots; that choice was made because such an apparatus could be built using known fabrication techniques, and described mathematically without gratuitous complications. In fact, our basic conclusions are known to be valid even when the assumption of low temperature is relaxed somewhat [11]. Direct measurement of the energy landscapes presented here, such as Fig. 2.7, is still a few years away because of the difficulty of verifying that groups of quantum dots share exactly the same shape and size [12].

1.2 Dissipative processes in semiconductor lasers

Photonic and spintronic devices are subjects of large-scale and ongoing research, because they are smaller and use less energy than circuit elements which operate by the gross motion of electrons. Heterostructure lasers using quantum wells (i.e. layers so thin that charge carriers

cannot move in a direction perpendicular to them, separated by doped buffers) benefit from the presence of III-V semiconductors: empirically, the laser's gain seems to increase with reduced dimensionality in that case [13], and population inversion occurs sooner when the band offsets between the active regions and the buffers are large [14, 15, 16].

Our initial aim in this area was to explain the results of particular experiments, but we were soon led to the more general issue of decoherence mechanisms in semiconductor lasers which are nearly always invoked heuristically rather than microscopically, such as spin exchange scattering by neutral impurities, and charge diffusion in microdisk structures. Chapters 3 and 4 attempt to treat these two phenomena in a more quantitative manner than has previously been achieved.

Chapter 2

Few-body spin couplings and their implications for universal quantum computation

2.1 Introduction

Electron spins in semiconductor quantum dots are a leading candidate for the physical realization of qubits in a quantum computer [10]. Although any quantum algorithm may be implemented using single-qubit and two-qubit gates [5], many such algorithms increase substantially in efficiency by exploiting simultaneous interactions among three or more qubits [17, 18, 19, 20, 21, 22, 23, 24, 25, 26, 27, 28, 29, 30]. In order to employ such simultaneous interactions, it is essential to understand in detail the many-body dynamics of the system of coupled qubits. More generally, since a practical quantum computer may need to contain as many as 10^6 qubits [26], it is essential to characterize the effect of many-body interactions on the system's overall energy landscape.

Previous studies [6, 11], using a model confining potential of superposed parabolic minima, demonstrated that three-body effects significantly influence the Hamiltonian of three electrons confined to three quantum dots at the vertices of an equilateral triangle, and that four-body effects are significant for four electrons confined to a tetrahedral arrangement of four dots. (The introduction of a third spin adds no new terms to the Hamiltonian, but the coupling strength for each pair of spins is changed non-trivially by the presence of the third.) Here we extend those results in two ways. Firstly, we analyze three quantum dots in a linear

geometry [31] and four dots in a square geometry [32], since these geometries are more likely to occur in a real experimental system. Secondly, by employing a Gaussian shape for the confining potential of each well [33], we explore the sensitivity of the many-body effects to the form of the confining potential. In both cases a nonperturbative calculation finds that many-body effects contribute appreciably to the Hamiltonian.

Hitherto, discussions of quantum dot quantum computation have nearly always assumed pairwise Heisenberg interactions. In view of the above result, this implies that computational errors may occur in the context of quantum computers using electron spin qubits in quantum dots, unless one always simultaneously couples only disjoint pairs of dots. There are at least four circumstances where this may be undesirable or even infeasible. One is fault tolerant quantum error correction, where simultaneous operations on several coupled dots has been associated with better error thresholds. A second is adiabatic quantum computation [29], in which the final Hamiltonian may include the simultaneous interactions that we discuss below. We will not analyze these applications here, although we believe that our methods are relevant to them.

We will focus on two other contexts, that of "encoded universality" (EU) [17, 18, 19, 20, 21], and that of computation on decoherence-free subspaces (DFSs) [17, 18, 34] and supercoherent qubits [30]. In these cases, the goal is to perform universal quantum computation using (in the case of EU) only the most easily controllable interaction or (in the cases of DFS and supercoherence) using only interactions that preserve the code subspace, since that subspace offers protection against certain types of decoherence. (Strong and fast exchange interaction pulses can further be used to suppress decoherence [35] and to eliminate decoherence-induced leakage [36].)

We will refer to these cases collectively as "encoded quantum computation". After establishing that four-body interaction terms can arise in a Heisenberg exchange Hamiltonian, we investigate the question of neutralizing their effect by using encoded qubits [17, 18, 20, 21, 30, 34, 35, 36, 37, 38, 39]. By generalizing the work of Bacon [40], who showed that universal quantum computation was possible using encoded gates with two-body coupling Hamiltonians (i.e. assuming that the Heisenberg Hamiltonian was applicable even when coupling three or more dots at a time), we enumerate tuning conditions on experimental parameters that are needed for the four-body effects to cancel out. An alternative is to design these encoded gates while allowing only pairs of electrons to couple at any given time. This is indeed possible, as shown in Ref. [41] for the price of significantly longer pulse

sequences per given encoded gate. Nevertheless, in view of the findings reported here and in Refs. [42, 43], this price may be worth paying.

2.2 Three-electron case

A system of three electrons within a confining scalar potential $V(\mathbf{r})$ obeys the Hamiltonian

$$H = \sum_{i=1}^{3}\left[\frac{\mathbf{p}_i^2}{2m} + V(\mathbf{r}_i)\right] + \sum_{i<j}\frac{e^2}{\kappa \mid \mathbf{r}_i - \mathbf{r}_j \mid} \tag{2.1}$$

$$\equiv \sum_{i=1}^{3} h(\mathbf{r}_i) + \sum_{i<j} w(\mathbf{r}_i, \mathbf{r}_j) \tag{2.2}$$

in the absence of spin-orbit coupling and external magnetic fields. Although Ref. [6] succeeded in demonstrating significant three-body and four-body effects in systems containing three or more electrons, a confining potential with quadratic minima has certain other characteristics which are unlikely to describe an experimental arrangement; for example, it diverges at large distances from the origin, and the single adjustable parameter ω_0 forces us to specify very narrow minima whenever we want a high barrier between them. We therefore begin with the Gaussian form

$$V(\mathbf{r}) = -V_0[e^{-\alpha|\mathbf{r}-\mathbf{A}|^2} + e^{-\alpha|\mathbf{r}-\mathbf{B}|^2} + e^{-\alpha|\mathbf{r}-\mathbf{C}|^2}], \tag{2.3}$$

which has two tunable parameters. The three fixed points are collinear and separated by a distance $2l$: $\mathbf{A} = (-2l, 0, 0)$, $\mathbf{B} = (0, 0, 0)$, and $\mathbf{C} = (2l, 0, 0)$.

We assume a Heitler-London approximation [44], wherein excited orbital states and states with double occupation of any single dot are neglected (see Ref. [43] for a recent discussion of the validity of this approximation in the context of electron spin qubits). The system's only degrees of freedom are therefore the spins of the confined electrons, leading to a total of $2^3 = 8$ "computational" basis states:

$$|\Psi(s_A, s_B, s_C)\rangle = \sum_P \delta_P P[|A\rangle\,|B\rangle\,|C\rangle\,|s_A\rangle\,|s_B\rangle\,|s_C\rangle]. \tag{2.4}$$

In the above, $|\{A\}\rangle$ are the three localized orbital ground states; $\left|s_{\{A\}}\right\rangle$ denote the corre-

sponding spin states; P is the set of all permutations of $\{A, B, C\}$; δ_P is 1 (-1) for even (odd) permutations. For instance, one of the eight (unnormalized) basis states is

$$\begin{aligned} |\Psi(\uparrow\uparrow\downarrow)\rangle &= |ABC\rangle\,|\uparrow\uparrow\downarrow\rangle - |ACB\rangle\,|\uparrow\downarrow\uparrow\rangle \\ &+ |CAB\rangle\,|\downarrow\uparrow\uparrow\rangle - |CBA\rangle\,|\downarrow\uparrow\uparrow\rangle \\ &+ |BCA\rangle\,|\uparrow\downarrow\uparrow\rangle - |BAC\rangle\,|\uparrow\uparrow\downarrow\rangle. \end{aligned}$$

To characterize the localized orbital state $|\{A\}\rangle$ for each dot, we expand (2.3) to quadratic order and solve the Schrödinger equation as though the other potential wells were absent:

$$\phi_A(\mathbf{r}) \equiv \langle \mathbf{r}|A\rangle \equiv \left(\frac{m\omega_o}{\pi\hbar}\right)^{3/4} \exp\left(-\frac{m\omega_o}{2\hbar}|\mathbf{r}-\mathbf{A}|^2\right). \tag{2.5}$$

Unless α is small compared to l^{-2}, this is of course a much coarser approximation than it would be for purely quadratic minima, so we refine it by centering $\phi_A(\mathbf{r})$ and $\phi_C(\mathbf{r})$ at the points which minimize $\langle A|h|A\rangle$ and $\langle C|h|C\rangle$. Because these orbitals overlap at least slightly for any finite ω_o, the states (2.4) are not orthogonal.

We now define H_{spin} to be the matrix representation of H in the basis (2.4), and expand it in terms of tensor products of Pauli matrices:

$$H_{\text{spin}} = \sum_{i,j,k} c_{ijk}\sigma_i \otimes \sigma_j \otimes \sigma_k.$$

This expansion is always possible, since the set of n-fold tensor products of Pauli matrices constitutes a complete orthonormal basis for the linear vector space of all $2^n \times 2^n$ matrices. Because we have written the basis (2.4) in the form $|s_A\rangle\,|s_B\rangle\,|s_C\rangle$, these Pauli matrices can be associated with spin operators on each of the three quantum dots. For example, we can write $\sigma_1 \otimes \sigma_3 \otimes \sigma_0 = 2S_{A,x} \otimes 2S_{B,z} \otimes I \equiv 4S_{A,x}S_{B,z}$, where the notation $S_{W,i}$ means the Pauli operator σ_i applied to the electron in the quantum dot at $\mathbf{W}$ and where I is the 2×2 identity matrix. (We exclude $\hbar$ from the definition of the matrices σ_i; thus, c_{ijk} have the dimensions of energy.) In the case of an arbitrary 8×8 matrix, 64 complex numbers would be required to specify c_{ijk} fully, but the operator (2.1) clearly has certain properties which constrain the values of the coefficients, such as Hermiticity, reflection symmetry, rotation symmetry, inversion symmetry, and invariance under permutation of the electrons' labels. Once these symmetries have been accounted for, the c_{ijk} may be characterized by just three

real quantities:

$$H_{\text{spin}} = K_0 + K_2[AB](\mathbf{S}_A \cdot \mathbf{S}_B + \mathbf{S}_B \cdot \mathbf{S}_C) + K_2[AC]\mathbf{S}_A \cdot \mathbf{S}_C, \tag{2.6}$$

where $\mathbf{S}_W \cdot \mathbf{S}_V = S_{W,x}S_{V,x} + S_{W,y}S_{V,y} + S_{W,z}S_{V,z}$ and $K_2[ij]$ is the pairwise coupling coefficient between the spins of the electrons in dots i and j. Here and elsewhere, we use symmetry considerations to reduce the number of coupling coefficients in our equations; in this case, the reflection symmetry of (2.3) through the x-z plane implies that $K_2[AB] = K_2[BC]$. Physically, the constant $K_2[AB]$ quantifies the coupling between adjacent spins, while $K_2[AC]$ describes the coupling between the spins at opposite ends of the row. (We note that Scarola et al. [42, 43] have shown that the application of a magnetic field breaks the inversion symmetry of the system, allowing chiral terms to arise in the spin Hamiltonian, also in addition to the naïve Heisenberg couplings.)

Defining $\mathbf{S}_{\text{T}} = \mathbf{S}_A + \mathbf{S}_B + \mathbf{S}_C$, one finds that

$$H_{\text{spin}} = L_0 + L_1\mathbf{S}_{\text{T}}^2 + L_1'(\mathbf{S}_A + \mathbf{S}_C)^2, \tag{2.7}$$

where

$$\begin{aligned} K_0 &= L_0 + \frac{9}{4}L_1 + \frac{3}{2}L_1' \\ K_2[AB] &= 2L_1 \\ K_2[AC] &= 2L_1 + 2L_1'. \end{aligned} \tag{2.8}$$

The expansion (2.7) reveals that any simultaneous eigenstate of $(\mathbf{S}_A + \mathbf{S}_C)^2$ and $\mathbf{S}_{\text{T}}^2$ is also an eigenstate of H_{spin}. We can construct such simultaneous eigenstates by using the Clebsch-Gordan table twice, first to combine the spin of the electron in dot A with the spin of the electron in dot C, and then to combine that spin-1 (or spin-0) system with the spin of the electron in dot B:

$$\begin{aligned} |\tfrac{3}{2}\ \tfrac{3}{2}\ ;\ 1\rangle &= |\Psi(\uparrow\uparrow\uparrow)\rangle \\ |\tfrac{3}{2}\ \tfrac{1}{2}\ ;\ 1\rangle &= |\Psi(\uparrow\uparrow\downarrow)\rangle + |\Psi(\uparrow\downarrow\uparrow)\rangle + |\Psi(\downarrow\uparrow\uparrow)\rangle \\ |\tfrac{3}{2}\ \text{-}\tfrac{1}{2}\ ;\ 1\rangle &= |\Psi(\downarrow\downarrow\uparrow)\rangle + |\Psi(\downarrow\uparrow\downarrow)\rangle + |\Psi(\uparrow\downarrow\downarrow)\rangle \\ |\tfrac{3}{2}\ \text{-}\tfrac{3}{2}\ ;\ 1\rangle &= |\Psi(\downarrow\downarrow\downarrow)\rangle \end{aligned} \tag{2.9}$$

$$
\begin{aligned}
|\tfrac{1}{2}\ \tfrac{1}{2}\ ;\ 1\rangle &= 2|\Psi(\uparrow\downarrow\uparrow)\rangle - |\Psi(\uparrow\uparrow\downarrow)\rangle - |\Psi(\downarrow\uparrow\uparrow)\rangle \\
|\tfrac{1}{2}\ \text{-}\tfrac{1}{2}\ ;\ 1\rangle &= 2|\Psi(\downarrow\uparrow\downarrow)\rangle - |\Psi(\downarrow\downarrow\uparrow)\rangle - |\Psi(\uparrow\downarrow\downarrow)\rangle \\
|\tfrac{1}{2}\ \tfrac{1}{2}\ ;\ 0\rangle &= |\Psi(\uparrow\uparrow\downarrow)\rangle - |\Psi(\downarrow\uparrow\uparrow)\rangle \\
|\tfrac{1}{2}\ \text{-}\tfrac{1}{2}\ ;\ 0\rangle &= |\Psi(\downarrow\downarrow\uparrow)\rangle - |\Psi(\uparrow\downarrow\downarrow)\rangle,
\end{aligned}
$$

where the indices on the left-hand side denote the values of $S_{\rm T}$, $S_{{\rm T},z}$, and $|\mathbf{S}_A + \mathbf{S}_C|$ respectively. Although the states $|\ \Psi(s_A, s_B, s_C)\rangle$ are not orthonormal, the eight states (2.9) are orthogonal, and they are also eigenvectors of the 8×8 matrix (2.7), which means that $H_{\rm spin}$ has been diagonalized. To obtain the parameters $\{L_0, L_1, L_1'\}$ we will choose three eigenstates with different good quantum numbers, and observe that their energies can be evaluated either by matrix algebra or by integrating microscopically over the axes $\mathbf{r}_i$ and the spins to compute the expectation value of (2.1):

$$
\langle\Psi|H_{\rm spin}|\Psi\rangle = \langle\Psi|H|\Psi\rangle. \tag{2.10}
$$

Inserting (2.7) into the left-hand side, for three distinct combinations of the good quantum numbers $\{(\mathbf{S}_A + \mathbf{S}_C)^2, S_{\rm T}^2\}$, yields

$$
\begin{aligned}
\frac{\langle\tfrac{3}{2}\ \tfrac{3}{2}\ ;\ 1\ |\ H_{\rm spin}\ |\tfrac{3}{2}\ \tfrac{3}{2}\ ;\ 1\rangle}{\langle\tfrac{3}{2}\ \tfrac{3}{2}\ ;\ 1\ |\tfrac{3}{2}\ \tfrac{3}{2}\ ;\ 1\rangle} &= L_0 + \frac{15}{4}L_1 + 2L_1' \\
\frac{\langle\tfrac{1}{2}\ \tfrac{1}{2}\ ;\ 1\ |\ H_{\rm spin}\ |\tfrac{1}{2}\ \tfrac{1}{2}\ ;\ 1\rangle}{\langle\tfrac{1}{2}\ \tfrac{1}{2}\ ;\ 1\ |\tfrac{1}{2}\ \tfrac{1}{2}\ ;\ 1\rangle} &= L_0 + \frac{3}{4}L_1 + 2L_1' \\
\frac{\langle\tfrac{1}{2}\ \tfrac{1}{2}\ ;\ 0\ |\ H_{\rm spin}\ |\tfrac{1}{2}\ \tfrac{1}{2}\ ;\ 0\rangle}{\langle\tfrac{1}{2}\ \tfrac{1}{2}\ ;\ 0\ |\tfrac{1}{2}\ \tfrac{1}{2}\ ;\ 0\rangle} &= L_0 + \frac{3}{4}L_1,
\end{aligned} \tag{2.11}
$$

while the corresponding wave functions (2.9) turn the right-hand side into

$$
\begin{aligned}
E_{\frac{3}{2},\frac{3}{2};1} &= \frac{\langle\Psi(\uparrow\uparrow\uparrow)|H|\Psi(\uparrow\uparrow\uparrow)\rangle}{\langle\Psi(\uparrow\uparrow\uparrow)|\Psi(\uparrow\uparrow\uparrow)\rangle} \\
E_{\frac{1}{2},\frac{1}{2};1} &= \frac{\langle\Psi(\uparrow\uparrow\downarrow)|H|\Psi(\uparrow\uparrow\downarrow)\rangle + 2\langle\Psi(\uparrow\downarrow\uparrow)|H|\Psi(\uparrow\downarrow\uparrow)\rangle - 4\langle\Psi(\uparrow\uparrow\downarrow)|H|\Psi(\uparrow\downarrow\uparrow)\rangle + \langle\Psi(\uparrow\uparrow\downarrow)|H|\Psi(\downarrow\uparrow\uparrow)\rangle}{\langle\Psi(\uparrow\uparrow\downarrow)|\Psi(\uparrow\uparrow\downarrow)\rangle + 2\langle\Psi(\uparrow\downarrow\uparrow)|\Psi(\uparrow\downarrow\uparrow)\rangle - 4\langle\Psi(\uparrow\uparrow\downarrow)|\Psi(\uparrow\downarrow\uparrow)\rangle + \langle\Psi(\uparrow\uparrow\downarrow)|\Psi(\downarrow\uparrow\uparrow)\rangle} \\
E_{\frac{1}{2},\frac{1}{2};0} &= \frac{\langle\Psi(\uparrow\uparrow\downarrow)|H|\Psi(\uparrow\uparrow\downarrow)\rangle - \langle\Psi(\uparrow\uparrow\downarrow)|H|\Psi(\downarrow\uparrow\uparrow)\rangle}{\langle\Psi(\uparrow\uparrow\downarrow)|\Psi(\uparrow\uparrow\downarrow)\rangle - \langle\Psi(\uparrow\uparrow\downarrow)|\Psi(\downarrow\uparrow\uparrow)\rangle}.
\end{aligned} \tag{2.12}
$$

The evaluation of these matrix elements and overlap integrals is a tedious, but straightforward procedure given the microscopic forms of H and $\psi(\mathbf{r})$ in (2.1), (2.3) and (2.5). Combining (2.8), (2.11), and (2.12), we thus compute K_0, $K_2[AB]$ and $K_2[AC]$ in terms of

ω_0 and the dimensionless system parameters

$$x_b \equiv \frac{\frac{1}{2}m\omega_0^2 l^2}{\frac{1}{2}\hbar\omega_0} = \frac{m\omega_0 l^2}{\hbar} \tag{2.13}$$

$$x_c \equiv \frac{e^2}{\kappa l \hbar\omega_0} \tag{2.14}$$

$$x_v \equiv \frac{2V_0}{\hbar\omega_0}. \tag{2.15}$$

Physically, these quantities give the characteristic energies of the system in terms of the energy of the orbital ground state (2.5). x_b represents the height of the potential barrier between wells, while x_c represents the equilibrium Coulomb repulsion potential and x_v is proportional to the individual well depth V_0.

Here and in the following section, we have estimated experimentally relevant values of x_b and x_c as is done in Ref. [10]. We assume that the width of the function (2.5), which is $2\sqrt{\hbar/m\omega_o}$, must be roughly equal to the separation between adjacent dots $2l$; using (2.13), we conclude that $x_b \approx 1$. For GaAs heterostructure single dots, $\kappa \approx 13$, $m^* \approx 0.067\ m_{\rm e}$, and $\hbar\omega_o \approx 3$ meV, which according to (2.14) means that $x_c \approx 1.5$.

A potential of the form (2.3) is most suitable for quantum computation when αl^2 is close to 1; if the inverted Gaussian decays too quickly in space, the spin coupling in the system becomes negligible, and if it decays too slowly, the local minima in V tend to coalesce at the center. Using $\frac{1}{2}\hbar\omega_o \sim 1$ meV, $V_0 \approx 3$ meV (from Ref. [10]), and our prior estimate of $x_c \approx 1.5$, we obtain the relation $x_b \approx x_v \sim 3$ by applying (2.13), (2.14), and (2.15). Noting that the parameter x_c has very little influence on any of the coupling constants over physically realistic ranges of x_b and x_v (and in any event depends on quantities, such as κ, which are difficult to tune experimentally), we henceforth set $x_c = 1.5$.

Fig. 2.1 shows the energy shift K_0 as a function of the system parameters $\{x_b, x_v\}$. As one might expect, this spin-independent quantity increases with increasing x_v and decreasing x_b (whenever ω_o decreases, there is greater orbital overlap and thus more Coulomb repulsion, irrespective of spin state). The coupling constants $K_2[AB]$ and $K_2[AC]$ are plotted in Fig. 2.2 and Fig. 2.3 respectively. We notice that they differ (which rules out the simple Heisenberg form $H_{\rm spin} = J\sum_{i<j}(\mathbf{S}_i \cdot \mathbf{S}_j)$), and that $K_2[AC]$ is only about an order of magnitude smaller than $K_2[AB]$ as we have confirmed by studying $K_2[AB](x_b, x_v)$ and $K_2[AC](x_b, x_v)$ on a logarithmic scale. In the context of quantum computation, this demonstrates that a nearest-neighbor approximation for the coupling between dots is insufficient (see also Ref. [43], where

a similar conclusion was reported using a low-energy Hubbard model with one electron per site).

2.3 Four-electron case

For the case of four quantum dots arranged in a square of side $2l$, our formalism is more complex in detail but identical in structure. We therefore describe the computation only in outline.

The confining potential in the coordinate Hamiltonian

$$H = \sum_{i=1}^{4} \left[\frac{\mathbf{p}_i^2}{2m} + V(\mathbf{r}_i) \right] + \sum_{i<j} \frac{e^2}{\kappa \mid \mathbf{r}_i - \mathbf{r}_j \mid} \tag{2.16}$$

now becomes

$$\begin{aligned} V(\mathbf{r}) = -V_0 \quad [\quad & e^{-\alpha|\mathbf{r}-\mathbf{A}|^2} + e^{-\alpha|\mathbf{r}-\mathbf{B}|^2} \\ + \quad & e^{-\alpha|\mathbf{r}-\mathbf{C}|^2} + e^{-\alpha|\mathbf{r}-\mathbf{D}|^2}], \end{aligned}$$

where $\mathbf{A} = (0, 2l, 0)$, $\mathbf{B} = (2l, 2l, 0)$, $\mathbf{C} = (2l, 0, 0)$, and $\mathbf{D} = (0, 0, 0)$. Our computational basis consists of 16 fully antisymmetrized vectors of the form

$$\begin{aligned} |\Psi(s_A, s_B, s_C, s_D)\rangle \quad = \quad & \sum_P \delta_P P[|A\rangle\,|B\rangle\,|C\rangle\,|D\rangle \\ & \otimes |s_A\rangle\,|s_B\rangle\,|s_C\rangle\,|s_D\rangle]. \end{aligned} \tag{2.17}$$

The form of $\phi(\mathbf{r})$ remains the same; to maintain the required geometrical symmetries while minimizing the one-body energies, we now shift all four localized orbital wave functions an equal distance toward the point $(l, l, 0)$.

Expanding H in terms of products of Pauli matrices, as in

$$H_{\text{spin}} = \sum_{i,j,k,\ell} c_{ijk\ell} \sigma_i \otimes \sigma_j \otimes \sigma_k \otimes \sigma_l,$$

we discover by applying the symmetries of (2.16) that four-body terms now appear with

nonzero coupling coefficients:

$$\begin{aligned} H_{\text{spin}} = K_0 \;&+\; K_2[AB](\mathbf{S}_A\cdot\mathbf{S}_B+\mathbf{S}_B\cdot\mathbf{S}_C \\ &\qquad +\mathbf{S}_C\cdot\mathbf{S}_D+\mathbf{S}_D\cdot\mathbf{S}_A) \\ &+\; K_2[AC](\mathbf{S}_A\cdot\mathbf{S}_C+\mathbf{S}_B\cdot\mathbf{S}_D) \\ &+\; K_4[ABCD][(\mathbf{S}_A\cdot\mathbf{S}_B)(\mathbf{S}_C\cdot\mathbf{S}_D) \\ &\qquad +(\mathbf{S}_B\cdot\mathbf{S}_C)(\mathbf{S}_D\cdot\mathbf{S}_A)] \\ &+\; K_4[ACBD](\mathbf{S}_A\cdot\mathbf{S}_C)(\mathbf{S}_B\cdot\mathbf{S}_D), \end{aligned} \tag{2.18}$$

where $K_4[ijk\ell]$ is the four-body coupling coefficient among the spins of the electrons in dots i, j, k and ℓ. Physically, the constant $K_2[AB]$ describes the pairwise coupling between adjacent spins, while $K_2[AC]$ describes the pairwise coupling between non-adjacent spins, $K_4[ABCD]$ describes four-body interactions emphasizing pairs of adjacent spins, and $K_4[ACBD]$ describes four-body interactions emphasizing pairs of non-adjacent spins. We define $S_{\text{T}} = \mathbf{S}_A+\mathbf{S}_B+\mathbf{S}_C+\mathbf{S}_D$, which leads us to

$$\begin{aligned} H_{\text{spin}} \;&=\; L_0 + L_1\mathbf{S}_{\text{T}}^2 + L_1'[(\mathbf{S}_A+\mathbf{S}_C)^2+(\mathbf{S}_B+\mathbf{S}_D)^2] \\ &\quad +L_2(\mathbf{S}_{\text{T}}^2)^2 + L_2'(\mathbf{S}_A+\mathbf{S}_C)^2(\mathbf{S}_B+\mathbf{S}_D)^2, \end{aligned} \tag{2.19}$$

where

$$\begin{aligned} K_0 &= L_0 + 3L_1 + 3L_1' + \frac{45}{2}L_2 + \frac{9}{4}L_2' \\ K_2[AB] &= 2L_1 + 24L_2 \\ K_2[AC] &= 2L_1 + 2L_1' + 24L_2 + 3L_2' \\ K_4[ABCD] &= 8L_2 \\ K_4[ACBD] &= 8L_2 + 4L_2'. \end{aligned} \tag{2.20}$$

Applying the Clebsch-Gordan table three times creates sixteen simultaneous eigenstates of $(\mathbf{S}_A+\mathbf{S}_C)^2$, $(\mathbf{S}_B+\mathbf{S}_D)^2$, and S_{T}^2. Inserting five of these states with different good quantum numbers into (2.10) yields five equations for the five unknowns $\{L_0, L_1, L_1', L_2, L_2'\}$ in terms of the eigenstate energies. As before, these energies may be expressed in closed form as functions of x_b, x_c, and x_v by integrating the right-hand side of (2.10) explicitly.

The energy shift K_0 for the square case is plotted in Fig. 2.4; as before, this constant is largest for strongly Coulomb-coupled dots separated by low potential barriers. Figs. 2.5, 2.6, 2.7, and 2.8 depict the coupling coefficients $K_2[AB]$, $K_2[AC]$, $K_4[ABCD]$, and $K_4[ACBD]$ respectively. The departure from the pairwise Heisenberg picture is even more pronounced here: we see that for physically relevant values of the parameters $\{x_b, x_v\}$ the four-body coefficient $K_4[ACBD]$ is of the same order of magnitude as the two-body coefficient $K_2[AC]$, while $K_4[ABCD]/K_2[AB] \sim 0.1$, as may be confirmed by plotting Figs. 2.5 through 2.8 on a logarithmic scale. Typically $K_4[ACBD]$ is opposite in sign to $K_2[AC]$, leading to a particularly important competition between the two-body and four-body interactions.

In order to confirm that the qualitative similarities between our final results and those of Ref. [6] were not artefacts of having made two broad changes to $V(\mathbf{r})$ rather than one, we also analyzed both the $N = 3$ and $N = 4$ dot geometries using a confining potential of superposed quadratic minima. The variation of the coupling coefficients, within experimentally relevant ranges of x_b and x_c (analogous to Figs. 2.1 through 2.8), strongly resembled that for the Gaussian potential in all cases.

2.4 Computing in the presence of four-body interactions using encoded qubits

We have shown that coupling three dots simultaneously quantitatively modifies the value of the spin exchange constant, and that coupling four dots simultaneously switches on a four-body interaction term of the form $K_4(\mathbf{S}_A \cdot \mathbf{S}_B)(\mathbf{S}_C \cdot \mathbf{S}_D)$ and its permutations. This conclusion appears to be robust under changes in dot geometry and in the confining potential. A natural question is whether there exist methods to cancel the four-body correction. The issue is particularly urgent when one considers encoded quantum computation (EQC). In many known constructions of universal gates for EQC [17, 18, 19, 20, 21, 30, 34, 35, 36, 37, 38, 39, 41] there arises the need to simultaneously couple several spins. One of the most popular codes, described in detail below, uses four spins per encoded or logical qubit [17, 18, 20, 21, 30, 34, 35, 36, 37, 38, 39]. For this code, universal computation requires that four spins be coupled at the same time using pairwise Heisenberg interactions. Hence a priori it appears that EQC using the four-qubit code suffers from a fundamental flaw. We now explore whether the four-qubit code may be implemented in such a way that each four-body

coupling is either cancelled or reduced to an overall phase. Our findings highlight problems that the four-body terms present in the context of EQC, and also provide an interesting perspective on how the four-body terms may need to be dealt with in general.

2.4.1 The code

We now describe the four-spin DFS code, first proposed in Ref. [37] in the context of providing immunity against collective decoherence processes (see Ref. [39] for a review). Let the singlet and triplet states of two electrons i, j be denoted as

$$
\begin{aligned}
|s\rangle_{ij} &\equiv |S=0, m_S=0\rangle = \frac{1}{\sqrt{2}}\left(|\Psi(\uparrow\downarrow)\rangle - |\Psi(\downarrow\uparrow)\rangle\right) \\
|t_-\rangle_{ij} &\equiv |S=1, m_S=-1\rangle = |\Psi(\downarrow\downarrow)\rangle \\
|t_0\rangle_{ij} &\equiv |S=1, m_S=0\rangle = \frac{1}{\sqrt{2}}\left(|\Psi(\uparrow\downarrow)\rangle + |\Psi(\downarrow\uparrow)\rangle\right) \\
|t_+\rangle_{ij} &\equiv |S=1, m_S=1\rangle = |\Psi(\uparrow\uparrow)\rangle.
\end{aligned}
$$

Then a single encoded DFS qubit is formed by the two singlets of four spins, i.e. the two states with zero total spin $S_{\mathrm{T}} = |\mathbf{S}_A + \mathbf{S}_B + \mathbf{S}_C + \mathbf{S}_D|$. These states are formed by combining two singlets of two pairs of spins ($|0_L\rangle$), or triplets of two pairs of spins ($|1_L\rangle$), with appropriate Clebsch-Gordan coefficients:

$$
\begin{aligned}
|0_L\rangle &= |s\rangle_{AB} \otimes |s\rangle_{CD} \\
&= \frac{1}{2}\left(|\Psi(\uparrow\downarrow\uparrow\downarrow)\rangle + |\Psi(\downarrow\uparrow\downarrow\uparrow)\rangle\right. && (2.21) \\
&\quad \left. -|\Psi(\uparrow\downarrow\downarrow\uparrow)\rangle - |\Psi(\downarrow\uparrow\uparrow\downarrow)\rangle\right) && (2.22) \\
|1_L\rangle &= \frac{1}{\sqrt{3}}\left(|t_-\rangle_{AB} \otimes |t_+\rangle_{CD} - |t_0\rangle_{AB} \otimes |t_0\rangle_{CD}\right. \\
&\quad \left. +|t_+\rangle_{AB} \otimes |t_-\rangle_{CD}\right) \\
&= \frac{1}{\sqrt{3}}(2|\Psi(\uparrow\uparrow\downarrow\downarrow)\rangle + 2|\Psi(\downarrow\downarrow\uparrow\uparrow)\rangle - |\Psi(\uparrow\downarrow\downarrow\uparrow)\rangle \\
&\quad -|\Psi(\downarrow\uparrow\uparrow\downarrow)\rangle - |\Psi(\uparrow\downarrow\uparrow\downarrow)\rangle - |\Psi(\downarrow\uparrow\downarrow\uparrow)\rangle). && (2.23)
\end{aligned}
$$

As shown in Refs. [17, 18], the Heisenberg interaction $\mathbf{S}_i \cdot \mathbf{S}_j$ can be used by itself to implement universal quantum computation on this type of system. The Heisenberg interaction is closely

related to the exchange operator E_{ij}, defined as

$$E_{ij} = \begin{pmatrix} 1 & & & \\ & 0 & 1 & \\ & 1 & 0 & \\ & & & 1 \end{pmatrix} \tag{2.24}$$

via $E_{ij} = \frac{1}{2}(4\mathbf{S}_i \cdot \mathbf{S}_j + I)$. The difference in their action as gates is only a phase; hence we will use E_{ij} and $\mathbf{S}_i \cdot \mathbf{S}_j$ interchangably from now on, and write $E_{ij} \simeq \mathbf{S}_i \cdot \mathbf{S}_j$. The E_{ij} have a simple action on the electronic spin basis states, as seen from the matrix representation (2.24): the states $|00\rangle$ and $|11\rangle$ are invariant whereas $|01\rangle$ and $|10\rangle$ are exchanged. Using this, it is simple to show that in the $\{|0_L\rangle, |1_L\rangle\}$ basis the exchange operators can be written as [18, 38]

$$\begin{aligned} E_{AB} = E_{CD} &= \begin{pmatrix} -1 & 0 \\ 0 & 1 \end{pmatrix} = -\bar{Z} \\ E_{AC} = E_{BD} &= \frac{\sqrt{3}}{2}\bar{X} + \frac{1}{2}\bar{Z} \\ E_{AD} = E_{BC} &= -\frac{\sqrt{3}}{2}\bar{X} + \frac{1}{2}\bar{Z}, \end{aligned} \tag{2.25}$$

where $\bar{X}, \bar{Z}$ are the encoded Pauli matrices σ_x, σ_z, i.e. the Pauli matrices acting on the $|0_L\rangle, |1_L\rangle$ states. It follows from the Euler angle formula

$$e^{-i\omega \mathbf{n}\cdot\boldsymbol{\sigma}} = e^{-i\beta\sigma_z} e^{-i\theta\sigma_x} e^{-i\alpha\sigma_z}$$

that one can perform all single encoded-qubit operations on the DFS states simply by switching the exchange interaction on and off. Note that the Euler angle formula is satisfied by any pair of non-parallel axes, although orthogonal axes may be more convenient. One can obtain an encoded σ_x operation by switching on two interactions simultaneously for the appropriate time intervals:

$$\bar{X} = -2\left(E_{AC} + \frac{1}{2}E_{AB}\right)/\sqrt{3} = \left(E_{AC} - E_{AD}\right)/\sqrt{3}.$$

Use of the Euler angle formula requires a Hamiltonian which is a sum of exchange terms with controllable coefficients $J_{ij}(t)$:

$$H_{\rm S} = \sum_{i<j} J_{ij}(t) E_{ij}.$$

This is achievable, e.g., by using local magnetic fields [10, 32, 33, 45, 46], ferroelectric gates [47], or optical rectification [48]. It is important to emphasize that the latter two methods do not require magnetic field control, hence overcoming at least in part the problems with EQC raised in Refs. [42, 43]. This is an important advantage with regard to EQC, which renders these exclusively electrical control methods distinctly preferable to those using magnetic fields. However, residual magnetic fields (e.g. due to nuclear spin impurities) may remain a problem, especially in the group III-V semiconductors such as GaAs [49]. In silicon-based architectures, this problem can be minimized by isotopic purification [50].

2.4.2 Effect of the four-body terms on a single encoded qubit

Let us now consider how the four-body terms act on the DFS code. Using the results above, we find that

$$(\mathbf{S}_A \cdot \mathbf{S}_B)(\mathbf{S}_C \cdot \mathbf{S}_D) \simeq E_{AB}E_{CD} = (-\bar{Z})^2 = I$$

where I is the identity operator. Also,

$$\begin{aligned} E_{AC}E_{BD} &= \left(\frac{\sqrt{3}}{2}\bar{X} + \frac{1}{2}\bar{Z}\right)^2 \\ &= \frac{1}{4}\left[3I + I + \sqrt{3}(\bar{X}\bar{Z} + \bar{Z}\bar{X})\right] = I, \end{aligned}$$

and similarly $E_{AD}E_{BC} = I$. Thus all fourth-order terms $(\mathbf{S}_i \cdot \mathbf{S}_j)(\mathbf{S}_k \cdot \mathbf{S}_l) \propto I$, as long we restrict their action to the subspace encoding one qubit. This implies that the encoding into the 4-qubit DFS is immune to the fourth-order terms. In other words, when this encoding is used, the problem of the computational errors induced by the undesired fourth-order terms simply disappears, as long as we restrict our attention to a single encoded qubit.

2.4.3 Two encoded qubits

We must also be able to couple encoded qubits via a non-trivial gate such as controlled-phase: $CP = \mathrm{diag}(-1, 1, 1, 1)$. This is one way to satisfy the requirements for universal quantum computation [51], though it is also possible to complete the set of single-qubit gates by measurement operators [52]. Two encoded qubits of the form (2.22), (2.23) occupy a four-dimensional subspace of the zero total spin subspace of eight spins. The zero total spin subspace is 14-dimensional. A very useful graphical way of seeing this, introduced in Ref. [18] but also known as a Bratteli diagram, is depicted in Fig. 2.9.

As more spins are added (horizontal axis), there are more possibilities for constructing a state with a given total spin (vertical axis). In the case of four spins there are two paths leading from the origin to $S_{\mathrm{T}} = 0$; these correspond exactly to the $|0_L\rangle$ and $|1_L\rangle$ code states. For eight spins there are 14 such paths. Only four of these correspond to the four basis states $\{|0_L0_L\rangle, |0_L1_L\rangle, |1_L0_L\rangle, |1_L1_L\rangle\}$. It is convenient to label paths according to the intermediate total spin: the state $|S_1, S_2, S_3, S_4, S_5, S_6, S_7, S_8\rangle$, where S_k is the total spin of k spin-1/2 particles, uniquely corresponds to a path in Fig. 2.9 (we omit the origin in this notation), and the S_k form a complete set of commuting observables [18]. For example,

$$|0_L0_L\rangle = |1/2, 0, 1/2, 0, 1/2, 0, 1/2, 0\rangle =$$

$$|0_L1_L\rangle = |1/2, 0, 1/2, 0, 1/2, 1, 1/2, 0\rangle =$$

$$|1_L0_L\rangle = |1/2, 1, 1/2, 0, 1/2, 0, 1/2, 0\rangle =$$

$$|1_L1_L\rangle = |1/2, 1, 1/2, 0, 1/2, 1, 1/2, 0\rangle =$$

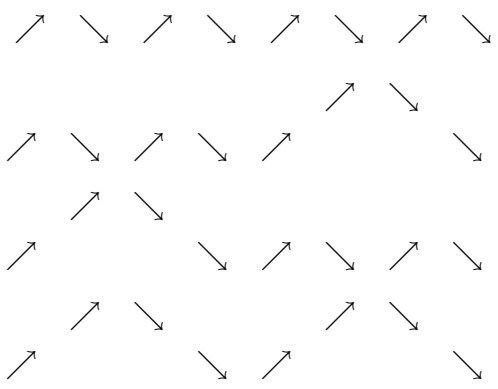

On the right, we have indicated the path in Fig. 2.9 corresponding to each state. The other 10 states with zero total spin can be similarly described. Thus the set of 14 states $\{|S_1, S_2, S_3, S_4, S_5, S_6, S_7, 0\rangle\}$ forms a basis for the subspace of zero total spin of eight spin-1/2 particles. Henceforth we will find it convenient to represent exchange operators in this basis. We will order the 14 basis states as follows: first the four code states $|0_L0_L\rangle, |0_L1_L\rangle, |1_L0_L\rangle, |1_L1_L\rangle$

as above, then

$$
\begin{aligned}
&|1/2,0,1/2,1,1/2,0,1/2,0\rangle, |1/2,1,1/2,1,1/2,0,1/2,0\rangle,\\
&|1/2,0,1/2,1,1/2,1,1/2,0\rangle, |1/2,1,1/2,1,1/2,1,1/2,0\rangle,\\
&|1/2,0,1/2,1,3/2,1,1/2,0\rangle, |1/2,1,3/2,1,1/2,0,1/2,0\rangle,\\
&|1/2,1,3/2,1,3/2,1,1/2,0\rangle, |1/2,1,3/2,2,3/2,1,1/2,0\rangle,\\
&|1/2,1,1/2,1,3/2,1,1/2,0\rangle, |1/2,1,3/2,1,1/2,1,1/2,0\rangle.
\end{aligned}
$$

E.g. in this basis the operator E_{DE} has the representation[1]

$$
E_{DE} = \begin{pmatrix}
\frac{1}{2} & & & \frac{\sqrt{3}}{2} & & & & & & & & & & & \\
& \frac{1}{2} & & & & \frac{\sqrt{3}}{2} & & & & & & & & & \\
& & \frac{1}{2} & & & & \frac{\sqrt{3}}{2} & & & & & & & & \\
& & & \frac{1}{2} & & & & \frac{\sqrt{3}}{2} & & & & & & & \\
\frac{\sqrt{3}}{2} & & & & -\frac{1}{2} & & & & & & & & & & \\
& \frac{\sqrt{3}}{2} & & & & -\frac{1}{2} & & & & & & & & & \\
& & \frac{\sqrt{3}}{2} & & & & -\frac{1}{2} & & & & & & & & \\
& & & \frac{\sqrt{3}}{2} & & & & -\frac{1}{2} & & & & & & & \\
& & & & & & & & 1 & & & & & & \\
& & & & & & & & & 1 & & & & & \\
& & & & & & & & & & \frac{1}{4} & \frac{\sqrt{15}}{4} & & & \\
& & & & & & & & & & \frac{\sqrt{15}}{4} & -\frac{1}{4} & & & \\
& & & & & & & & & & & & 1 & & \\
& & & & & & & & & & & & & 1 &
\end{pmatrix}.
$$

Recall that the first four rows refer to the code space. It is then clear that E_{DE} mixes the code space with four of the remaining ten states that have zero total spin. This is a general feature of all exchange operators acting on two code blocks simultaneously. For this reason it is impossible to couple two code blocks in one step while preserving the code space.

[1] All matrix calculations reported here and in the Appendix were performed with Mathematica.

2.4.4 Enacting an encoded controlled-phase gate

For the four-qubit code above, procedures implementing a CP gate were first given in Refs. [17, 18]. Recently, Bacon [40, Appendix E] has found a simplified scheme which is a useful starting point for our purposes. Bacon's implementation of a CP gate between two pairs of four-qubit blocks (qubits A-D and qubits E-H) involves a sequence of 14 elementary gates, each of which requires that several simultaneous exchange interactions be switched on and off. In the following calculation, we will employ Bacon's construction, with some adjustments to compensate for three- and four-body corrections. For ease of visualization we will assume that the two blocks are squares of side $2l$ and that dots D and E are separated by a distance $2l$, although nearly all of the following calculations are independent of the exact spatial relationship between the blocks.

The gates are (adapting the notation of Ref. [40])

$$
\begin{aligned}
U_1 &= \exp\left\{\frac{i\pi}{\sqrt{3}}\left[E_{DE} + \frac{1}{2}\sum_{A=i<j}^{D} E_{ij}\right]\right\} \\
U_2 &= \exp\left\{\frac{i\pi}{4\sqrt{2}}\left[-3E_{EF} - \frac{2}{3}\left(E_{FG} + E_{FH} + E_{GH}\right)\right]\right\} \\
U_3 &= \exp\left\{\frac{i\pi}{4\sqrt{2}}\left[-3E_{CD} - \frac{2}{3}\left(E_{AB} + E_{AC} + E_{BC}\right)\right]\right\} \\
U_5 &= \exp\left\{\frac{i\pi}{\sqrt{3}}\left[E_{FG} + \frac{1}{2}E_{GH}\right]\right\} \\
U_6 &= \left(U_A U_B U_A^\dagger U_B^\dagger\right)^2,
\end{aligned}
$$

where

$$
\begin{aligned}
U_A &= \exp\left[-\frac{i}{2}\cos^{-1}(-1/3)E_{DE}\right] \\
U_B &= \exp\left[-\frac{i\pi}{2}\sum_{A=i<j}^{D} E_{ij}\right].
\end{aligned}
$$

In terms of these gates the controlled-phase gate can be written as

$$
CP = U_1^\dagger (U_2^\dagger U_3^\dagger) U_5^\dagger U_6 U_5 (U_3 U_2) U_1, \tag{2.26}
$$

where U_3U_2 can be executed in one step since by inspection the two gates operate on the two blocks separately. This gate sequence operates in the entire 14-dimensional subspace of $S_{\rm T} = 0$ states of eight spins: the system leaves the code space after the application of U_1, but returns to it at the end of the sequence when $U_1^\dagger$ is applied. Hence our single-qubit considerations above do not apply: even if a four-body interaction acts as the identity operator on a single encoded qubit, it may act non-trivially in the larger $S_{\rm T} = 0$ space. We must therefore carefully analyze the action of this gate sequence in light of the three- and four-body corrections.

The key idea in Bacon's construction of the gate sequence is to ensure that each gate acts "classically", i.e. it only couples a given $S_{\rm T} = 0$ basis state to another without creating superpositions of such basis states (that the gates above act in this manner is not at all simple to see directly, but is the reason for the particular choice of angles in the gates). We find that, in order to maintain this key condition, it is necessary to tune the four-body exchange coupling constants during the computation. Thus to enact a CP gate in the presence of four-body interactions, the experimental apparatus requires a certain amount of flexibility. We note that there are other ways to obtain a CP gate [41]; our present goal is mainly to explore the implications of the four-body terms in a context of some general interest.

A detailed matrix calculation (see Appendix) shows us that the effect of nearly every gate in (2.26) depends upon the relative strengths of the exchange coefficients between the various pairs or quartets of dots it couples, as in

$$CP' = U_1'^\dagger(J_a', J_b', J_c', J_d') \left[U_2'^\dagger(J_2') U_3'^\dagger(J_3')\right] U_5'^\dagger U_6'(J_B') U_5' \left[U_3'(J_3') U_2'(J_2')\right] U_1'(J_a', J_b', J_c', J_d')$$

where the parameters $\{J\}$ are determined by the shapes and strengths of the individual dot confining potentials. Comparison with the results of Ref. [40] then yields the following relations between these new coefficients:

1. The constant J_c' can take on an arbitrary value.

2. The constants J_2' and J_2'' must be chosen to satisfy the transcendental equation $\eta = 0$ (see Appendix).

3. The constants J_3' and J_3'' must be chosen to satisfy the transcendental equation $\eta = 0$ (see Appendix).

4. The constant J_5' must either be zero or chosen such that $\sqrt{\frac{4}{3}(J_5')^2 - 2J_5' + 1}$ is an even integer.

5. The constant J_B' must be an integer.

6. The constants J_a', J_b', J_d' can take on an infinite set of rationally related values, wherein the ratio of any pair (such as J_b'/J_d') can be chosen completely arbitrarily and the value of the third constant is determined by this choice.

The most restrictive of these conditions is that J_B' must be an integer. Since the gates are applied sequentially, however, this condition need only be satisfied during the application of the U_6' gate, and it is plausible from the earlier sections of this chapter that corresponding Heisenberg exchange constants can be found. When these conditions are satisfied it is indeed the case that $CP' = (-1, 1, 1, 1)$ on the code space.

2.4.5 Dimensionality of parameter spaces required by two-body and four-body couplings

We caution that, although the encoding procedure described above has been shown mathematically to remove the effect of the four-body couplings, the experimental construction of a suitable apparatus using real quantum dots is another matter, as the following heuristic calculation suggests.

Our modified gates imply the following constraints on the coupling coefficients (see Appendix for the definitions of Λ and η):

$\underline{U_5' \text{ gate}}$

(a) $K_2[FG] = \frac{1}{2}K_2[GH]$;

(b) Either $K_2[FH] = 0$ or $\Lambda(K_2[FH]) = 2n$, where n must have an integer value;

$\underline{U_B' \text{ gate}}$

(c) $K_2[ij]$ is the same for all pairs within $\{A, B, C, D\}$;

(d) $K_4[ABCD] = K_4[ACBD] = K_4[ADBC]$;

(e) $K_4[ABCD] = 2mK_2[AB]$, where m may have any integer value;

$\underline{U_2' \text{ gate}}$

(f) $K_2[FG] = K_2[FH] = K_2[GH]$;

(g) $K_2[EF] = \frac{9}{2}K_2[GH]$;

(h) $K_4[EGFH] = K_4[EHFG]$;

(i) Either $K_4[EFGH] = K_4[EGFH]$, or $K_4[EFGH]$ and $K_4[EGFH]$ satisfy the transcendental equation $\eta(K_4[EFGH], K_4[EGFH]) = 0$;

$\underline{U_3' \text{ gate}}$

(j) $K_2[AB] = K_2[AC] = K_2[BC]$;

(k) $K_2[CD] = \frac{9}{2}K_2[AB]$;

(l) $K_4[ACBD] = K_4[ADBC]$;

(m) Either $K_4[ABCD] = K_4[ACBD]$, or $K_4[ABCD]$ and $K_4[ACBD]$ satisfy the transcendental equation $\eta(K_4[ABCD], K_4[ACBD]) = 0$;

$\underline{U_1' \text{ gate}}$

(n) $K_2[ij]$ is the same for all pairs within $\{A, B, C, D\}$;

(o) $K_2[DE] = 2K_2[AB]$;

(p) $K_4[ABCD] = K_4[ACBD] = K_4[ADBC]$;

(q) $K_4[ABCE] = K_4[ACBE] = K_4[AEBC]$;

(r) $K_4[ADBE] = K_4[AEBD]$;

(s) $K_4[ADCE] = K_4[AECD]$;

(t) $K_4[BDCE] = K_4[BECD]$;

(u) $K_4[ADBE] = K_4[ADCE] = K_4[BDCE]$;

(v) $K_4[ABDE]$ is a certain single-valued function of $K_4[ADBE]$;

(w) $K_4[BCDE]$ is a certain single-valued function of $K_4[ADCE]$;

(x) $K_4[ACDE]$ is a certain single-valued function of $K_4[BDCE]$.

Since the coupling coefficients must in general vary with time in order to satisfy all of these constraints (for example, $K_2[CD]$ and $K_2[AC]$ would be equal during the operation of U'_B but unequal during U'_3), we also assume that groups of constraints need be concurrently satisfied only when they arise from the same gate.

We first note that, by the same reasoning used to derive (2.6) and (2.18), a four-dot Hamiltonian for the geometry of $\{A, B, C, E\}$ contains a constant term and 9 independent coupling coefficients. If these 9 coefficients assumed a given set of values and we wished to adjust them to meet constraints such as those listed above, we would need 9 additional degrees of freedom in the system. We make the conservative assumption, however, that one two-body coefficient and one four-body coefficient can be left unaltered and the others adjusted to correspond to them, which means that only 7 additional parameters are required. Similarly, for the subset $\{A, B, D, E\}$ ($\{A, C, D, E\}$, $\{B, C, D, E\}$, $\{A, B, C, D\}$), there are 9 (6, 7, 5) independent coupling coefficients for which we require 7 (4, 5, 3) tunable parameters if a given set of constraints are to be satisfied. We will of course count one more degree of freedom when a constraint includes relationships between the two-body and four-body energies.

Now suppose that we designate one "baseline" choice of $\{x_b, x_c, x_v\}$ such that within each of the two squares, all the quantities $K_2[ij]$ are equal, all the quantities $K_4[ijkl]$ are equal, and $K_4[ijkl] = 2K_2[ij]$. That arrangement can simultaneously satisfy constraints (b), (c), (d), (e), (f), (h), (i), (j), (l), (m), (n), and (p) provided that the value of $K_2[FH]$ is chosen appropriately. From this potential, we would need to make one change within $\{E, F, G, H\}$ to reach condition (a) or condition (g), or one other change within the second quartet of dots to obtain (k) or (o). The couplings of $\{A, B, C, E\}$ must be adjusted to match (q) while still satisfying (n), (o), and (p), which requires 6 additional degrees of freedom as explained in the preceding paragraph. Similarly, (v) ((w), (x)) and (r) ((s), (t)) together imply particular adjustments to the four-body couplings in $\{A, B, D, E\}$ ($\{A, C, D, E\}$, $\{B, C, D, E\}$) which require 6 (3,4) new parameters. (The single-valued function in question is the same for all three cases, so in the end $K_4[ABDE]$ is the same as $K_4[ACDE]$ and $K_4[BCDE]$.) Finally,

we need two more degrees of freedom available somewhere in order to meet constraint (u), for a grand total of 28 degrees of freedom.

To put the size of this number into perspective we also count the independently tuned energies necessary to meet the conditions on EQC using pairwise couplings alone. By choosing a suitable combination $\{x_b, x_c, x_v\}$ for an entire eight-spin system, we could satisfy (b), (c), (f), (j), and (n) at the same time; one more degree of freedom would be necessary to also satisfy (o). Starting from such a system we could presumably satisfy (a) or (g) by adjusting one parameter within $\{E, F, G, H\}$, or satisfy (k) by adjusting one parameter within $\{A, B, C, D\}$. Hence we estimate that 7 degrees of freedom are required for the purely Heisenberg Hamiltonian considered in Ref. [40].

We see that, even if one presupposes the ability to create and position many identical qubits of the form (2.22), (2.23) (3 free parameters), accounting correctly for two-body and four-body coupling is still a great deal more demanding than two-body coupling alone. In the model system of sections 2.2 and 2.3, these degrees of freedom correspond to changes in the shape of the static potential $V(\mathbf{r})$, but in other experimental proposals they might represent, e.g., the strengths of photon couplings between delocalized electron states [53], or the frequencies of EM fields which modulate interactions between nuclear spins [54]. As previously noted, the scalability of any of the proposed qubit implementations remains an open question; it may be that the number of tunable parameters can never be inflated in this manner without qualitative technological advances. It is this experimental challenge that must be weighed against the increased length (and hence vulnerability to decoherence) of pulse sequences employing only two-body couplings [41].

2.5 Summary and conclusions

Earlier work [6, 11] showed that in highly symmetrical geometries the interaction between three and four mutually interacting electrons confined in parabolic potentials contains many-body terms, which in the case of four electrons qualitatively modify the usual Heisenberg interaction. In this work we have improved upon these early results by considering realistic linear and square geometries and by utilizing Gaussian confining potentials. Specifically, we have shown in a Heitler-London calculation that in the case of four mutually interacting electrons, the system's Hamiltonian contains many-body exchange terms which may be comparable in size to the Heisenberg exchange interactions. This can have important implica-

tions for quantum information processing using coupled quantum dots. We have considered, in particular, the implications for quantum computation using logical qubits encoded into decoherence-free subspaces of four electrons per qubit. We showed that previously designed conditional quantum logic gates between these encoded qubits must be modified, in order to account for the four-body terms, when four or more electrons are coupled simultaneously. This requires the ability to tune, to a certain extent, the four-body exchange constants. It is worth noting, however, that there are alternatives to this method of implementing encoded conditional logic gates which may be less demanding. In particular, it is worth exploring the possibility of completing the set of universal encoded quantum logic gates by supplementing single-qubit gates (where, as we have shown, four-body effects are harmless) with measurements and teleportation, as in linear optics quantum computing [52]. This will be a subject for future research.

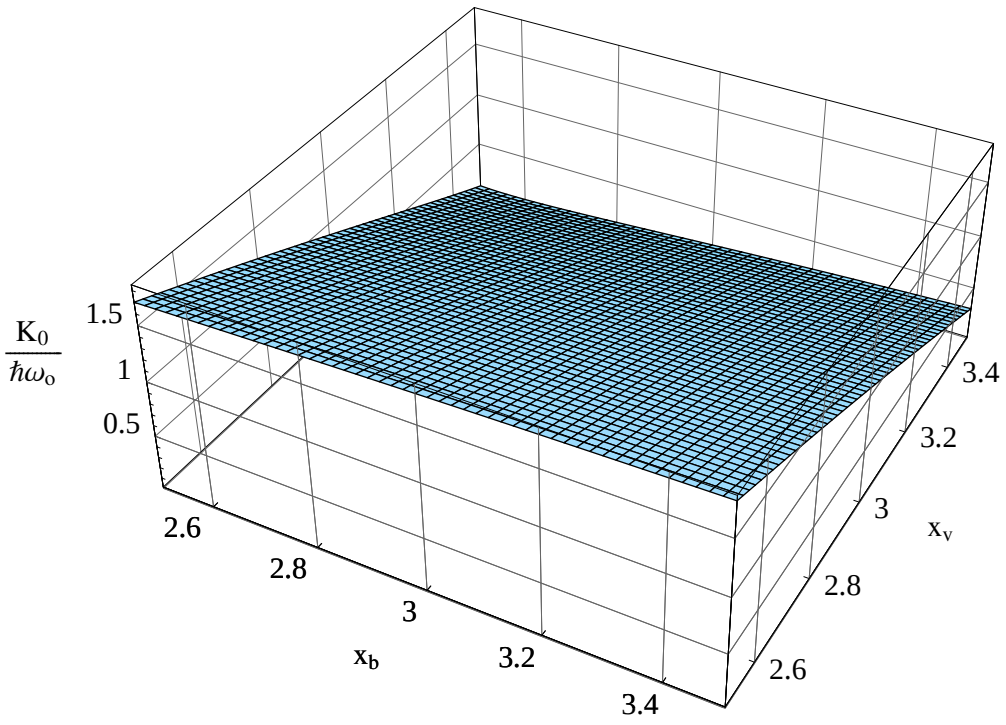

Figure 2.1. Plot of K_0, the overall energy shift, as a function of dimensionless barrier height x_b and overall well depth x_v in the case of three mutually interacting electrons in a linear geometry. In this and subsequent figures the Coulomb repulsion parameter x_c is set to 1.5 as in Ref. [6].

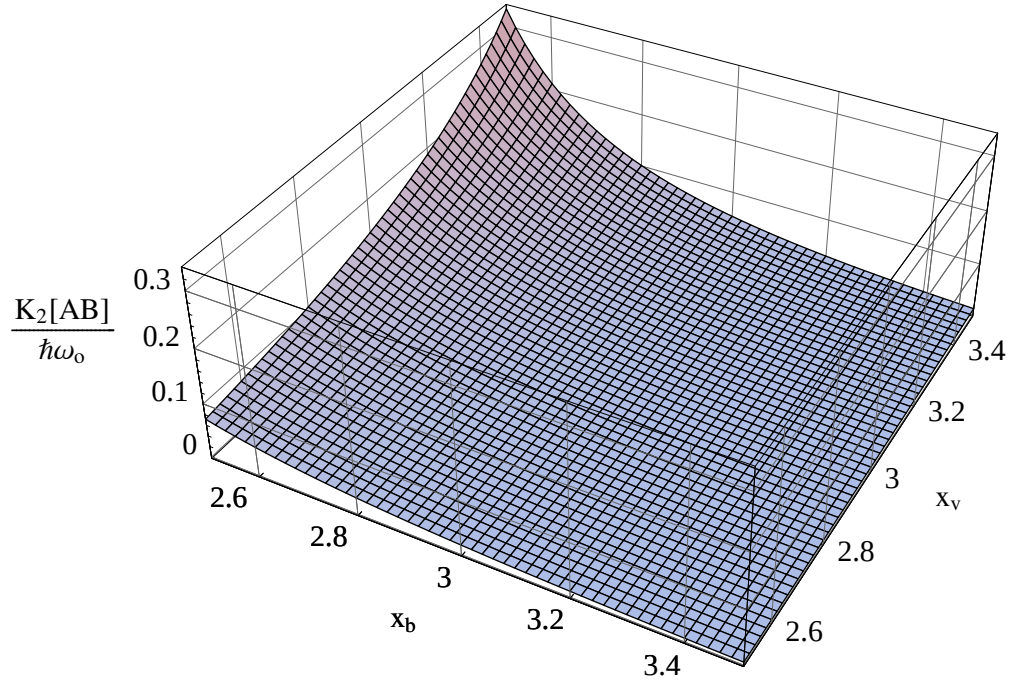

Figure 2.2. Plot of $K_2[AB]$, the two-body coupling coefficient for adjacent dots, as a function of dimensionless barrier height x_b and overall well depth x_v in the case of three mutually interacting electrons in a linear geometry.

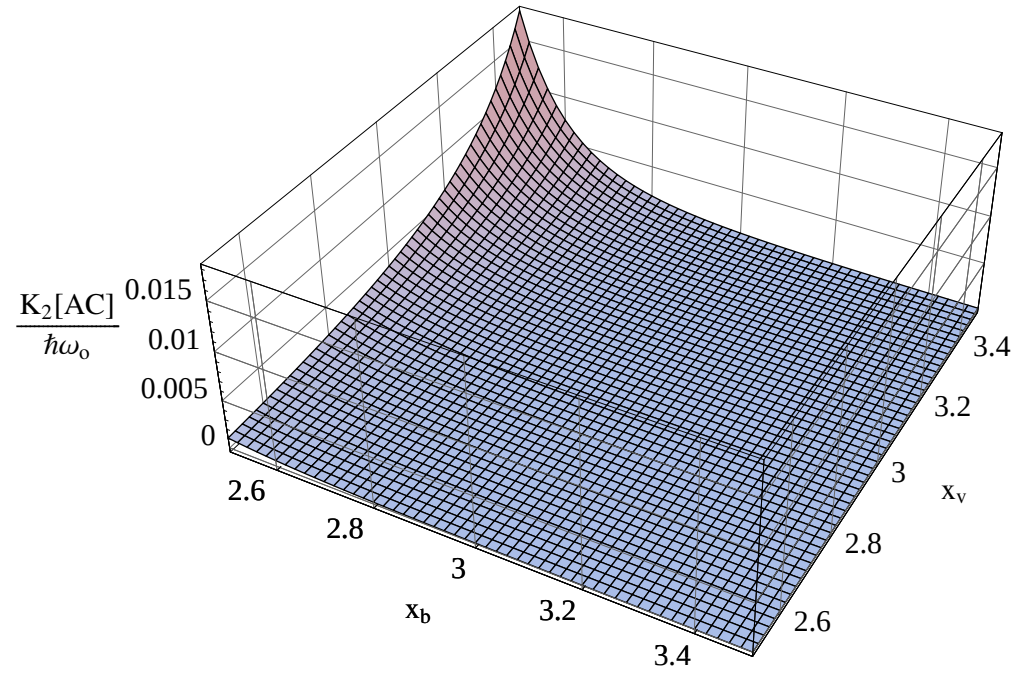

Figure 2.3. Plot of $K_2[AC]$, the two-body coupling coefficient for non-adjacent dots, as a function of dimensionless barrier height x_b and overall well depth x_v in the case of three mutually interacting electrons in a linear geometry.

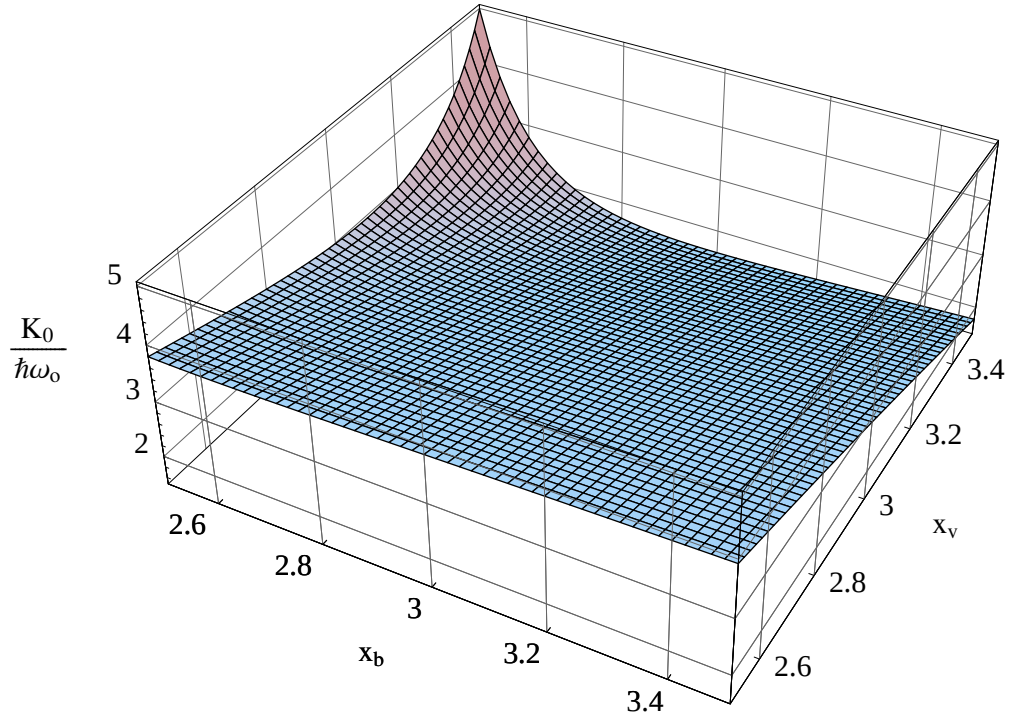

Figure 2.4. Plot of K_0, the overall energy shift, as a function of dimensionless barrier height x_b and overall well depth x_v in the case of four mutually interacting electrons in a square geometry.

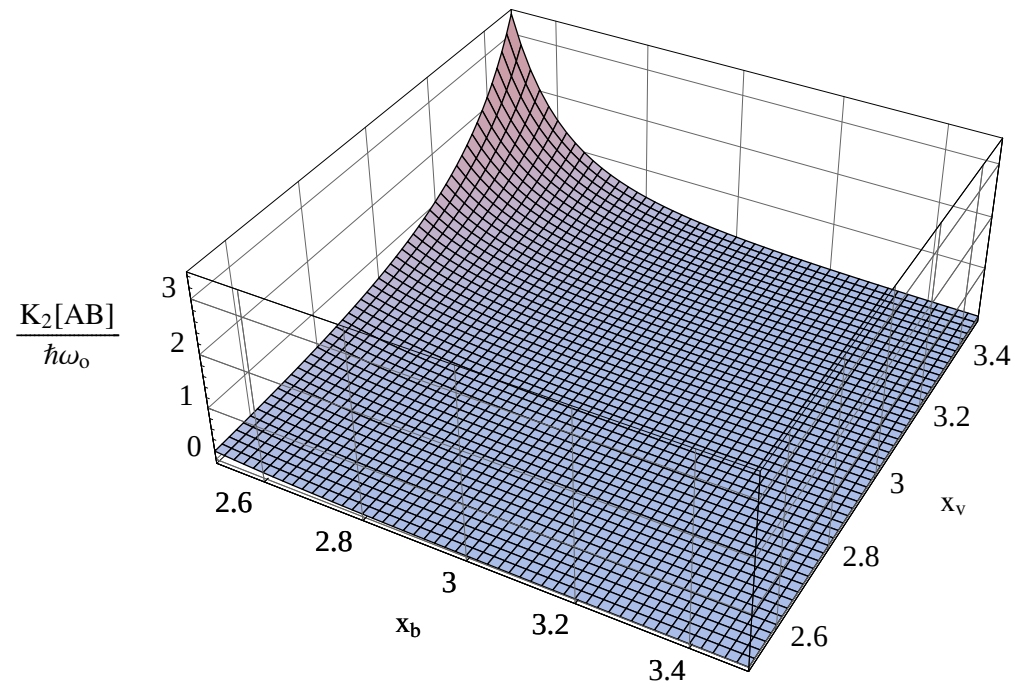

Figure 2.5. Plot of $K_2[AB]$, the two-body coupling coefficient for adjacent dots, as a function of dimensionless barrier height x_b and overall well depth x_v in the case of four mutually interacting electrons in a square geometry.

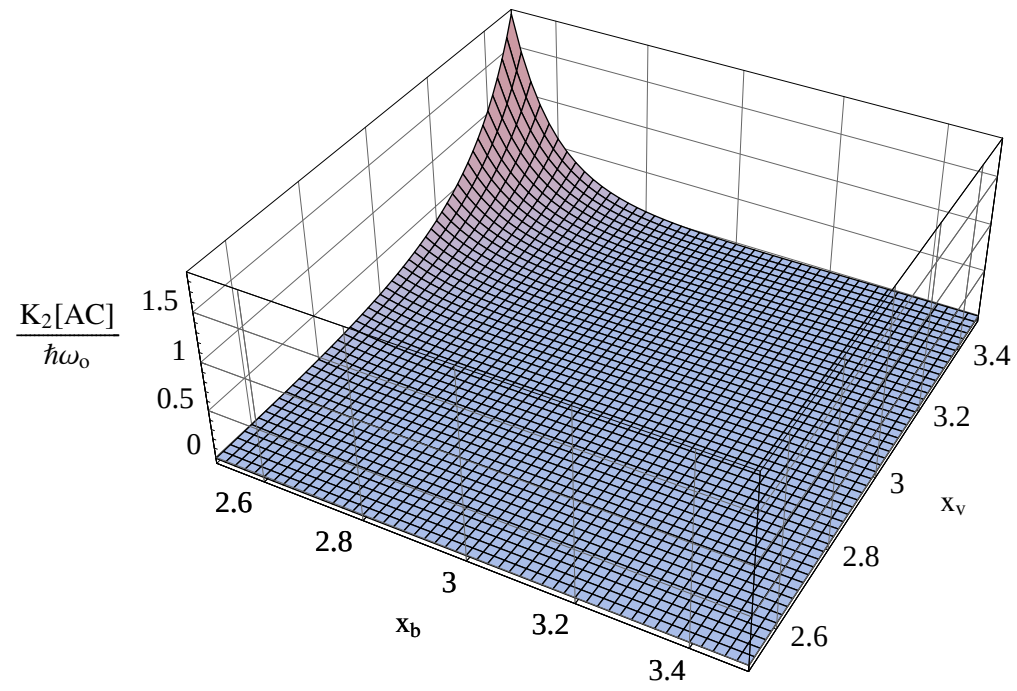

Figure 2.6. Plot of $K_2[AC]$, the two-body coupling coefficient for non-adjacent dots, as a function of dimensionless barrier height x_b and overall well depth x_v in the case of four mutually interacting electrons in a square geometry.

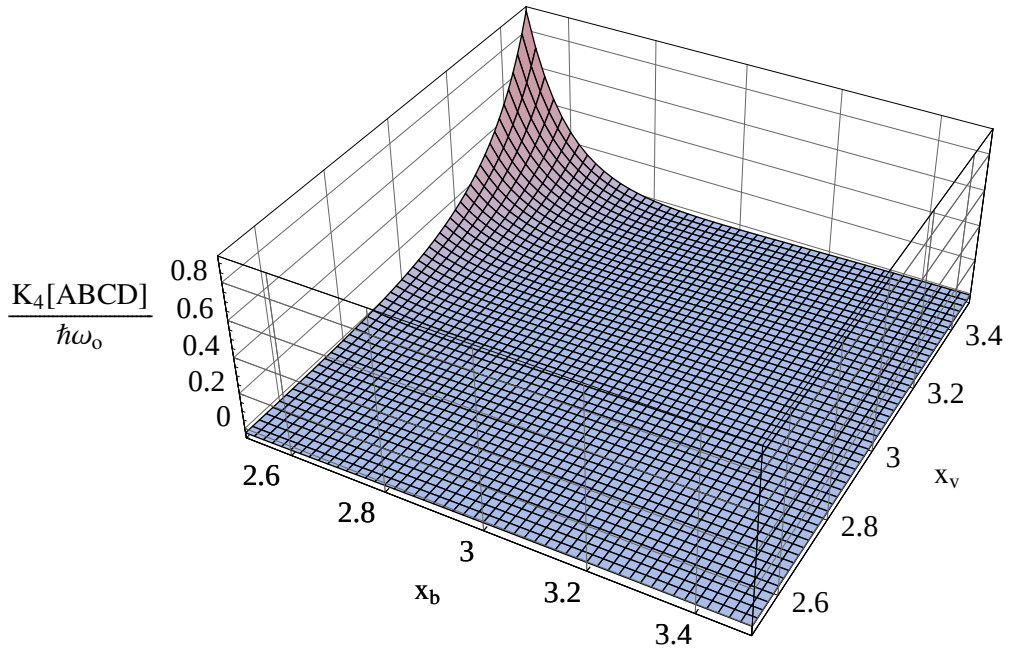

Figure 2.7. Plot of $K_4[ABCD]$, the four-body coupling coefficient for pairs of adjacent dots, as a function of dimensionless barrier height x_b and overall well depth x_v in the case of four mutually interacting electrons in a square geometry.

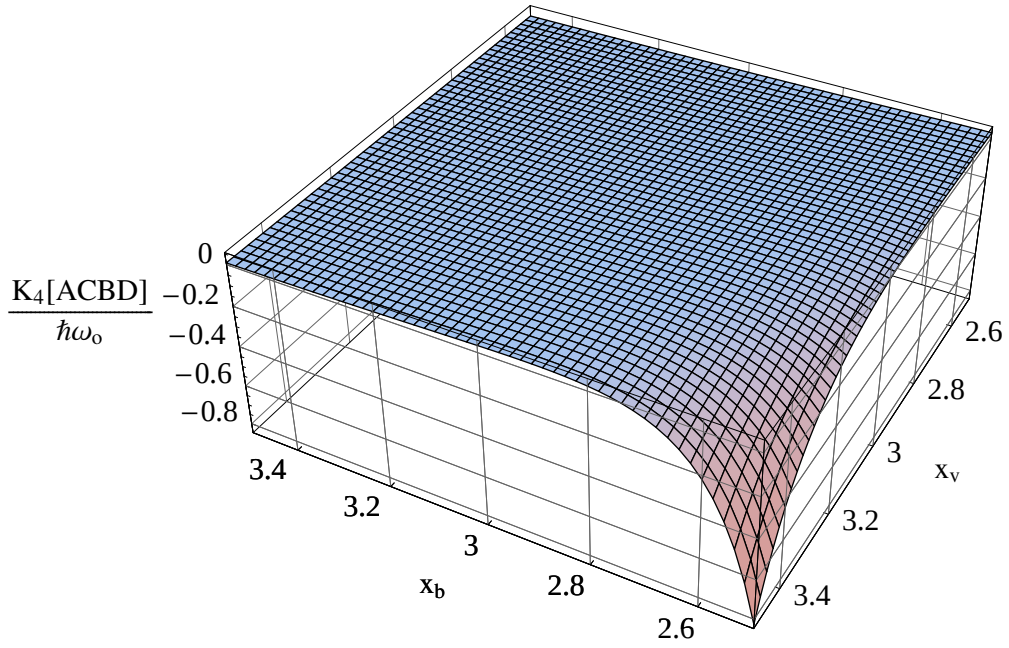

Figure 2.8. Plot of $K_4[ACBD]$, the four-body coupling coefficient for pairs of non-adjacent dots, as a function of dimensionless barrier height x_b and overall well depth x_v in the case of four mutually interacting electrons in a square geometry. Note that two of the axis directions are reversed from the preceding figures.

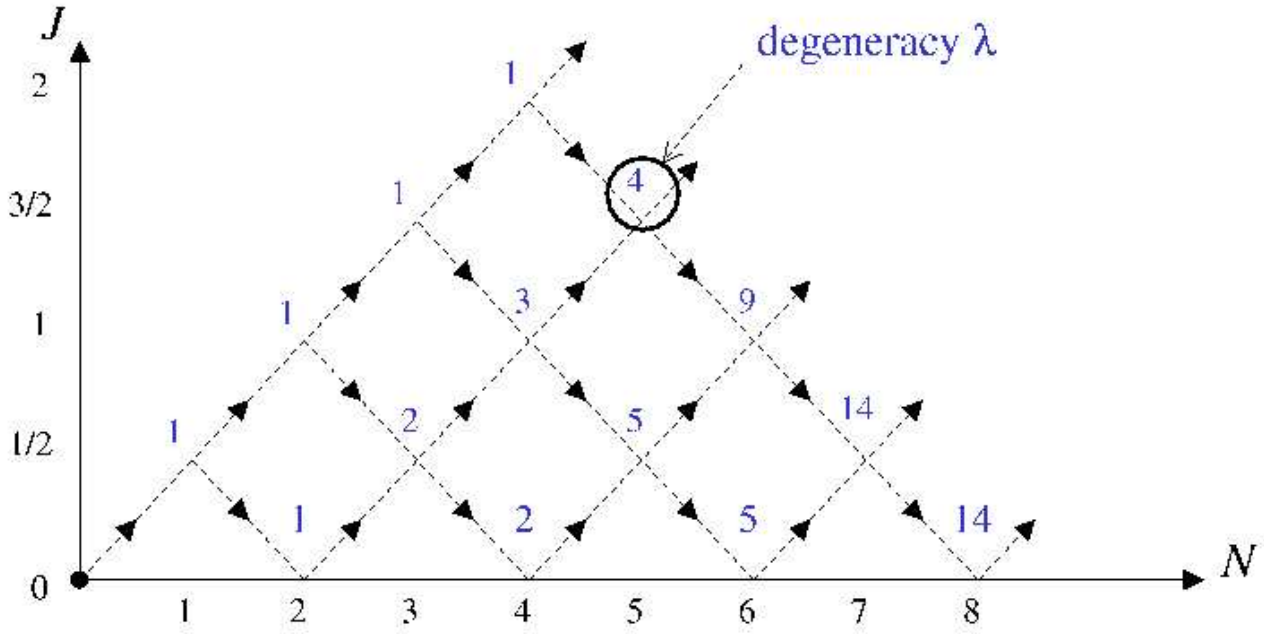

Figure 2.9. Partitioning of the Hilbert space of N spin-1/2 particles into decoherence-free subspaces (nodes of the graph). The integer above each node represents the number of paths leading from the origin to that node.

Chapter 3

Spin exchange scattering in semiconductors

3.1 Introduction

There is great interest in the field of spintronics: spin currents may conceivably be used to supplement or replace a variety of charge transport processes [55, 56, 57, 58, 59]. In all these devices, spin relaxation time is a central engineering consideration. Spin coherence is also important for many optical experiments [60, 61, 62, 63]. A rigorous theory of spin-flip scattering was presented by D'yakonov and Perel' [64], based on an earlier theory by Dresselhaus [65]. It uses the spin-orbit interaction, and is a small relativistic effect.

Our present goal is to calculate the rate of spin exchange scattering of conduction band electrons from electrons bound to neutral donors. If the bound electron initially has the opposite spin of the band electron, exchange scattering effectively flips the spin of the conduction electron. A similar process is the spin exchange scattering from an electron that is part of an exciton. The identical process can happen for holes, when they scatter from other holes bound to acceptors or excitons. These phenomena are not based on a relativistic process and, as we will see, create a much larger effect: the mean lifetimes we find are much shorter.

Electron scattering from neutral donors was investigated years ago in relation to the mobility of electrons and holes in semiconductors [66, 67, 68, 69]. That work used a variety of methods, including variational techniques [67], resonance scattering [68], and phase shifts [69]. It was assumed that the system had only two electrons, and thence the cross section

was computed for the spin singlet and spin triplet arrangements. If however one constructs many-electron eigenfunctions, for large numbers of band electrons and bound electrons, then each pair does not have the singlet-triplet symmetry. For that reason, our calculation differs from those in the earlier papers.

In metals, spin-flip scattering of a band electron by a localized electron is a well-known process [70, 71]. It causes the Kondo effect [70], among other phenomena. There the process is characterized by an effective interaction strength $V_{sd} = J\vec{S} \cdot \vec{s}$, where J is the interaction, and the two factors $\vec{s}, \vec{S}$ are the local spin and the band electron spin.

Here we use the Born approximation [72] to calculate J using hydrogen-like wave functions in two and three dimensions. Three-dimensional results are of interest for bulk devices; other applications involve quantum wells or superlattices, where the electron motion is largely two-dimensional. We find that the cross section for scattering has a very large dependence on the energy of the band electron, as well as varying with the density n_B of scattering centers (i.e. the density of donors).

3.2 Rate equations

The spin exchange scattering will cause a mutual spin flip between a bound spin and a conduction band spin, provided they have opposite initial spin states. Later, they can flip back. So we need to consider the rate equations for time-resolved spin polarization. Let $n_\sigma(t)$ be the density of conduction band spins with ($\sigma = \uparrow, \downarrow$), where the axis defining up and down is arbitrary. The total conduction band density $n = n_\uparrow + n_\downarrow$ is independent of time. Similarly, let $n_{B\sigma}(t)$ be the density of electron spins bound to donors. The sum $n_B = n_{B\uparrow} + n_{B\downarrow}$ is constant. In the following sections we employ Fermi's golden rule to calculate the rate γ of spin flip by the exchange process: γ has the dimensions of (length)^d/sec, where d is the dimensionality. Then the rate equations for the evolution of spin polarization are

$$\frac{d}{dt} n_\uparrow(t) = -\gamma[n_\uparrow(t) n_{B\downarrow}(t) - n_\downarrow(t) n_{B\uparrow}(t)] \tag{3.1}$$

$$= -\frac{d}{dt} n_\downarrow(t) = \frac{d}{dt} n_{B\downarrow}(t) = -\frac{d}{dt} n_{B\uparrow}(t). \tag{3.2}$$

The nonlinear equation (3.1) has a simple solution. Define the fractional magnetizations $m(t)$ for conduction electrons and $m_B(t)$ for bound electrons:

$$n_\uparrow(t) = \frac{n}{2}[1+m(t)], \quad n_{B\uparrow}(t) = \frac{n_B}{2}[1+m_B(t)] \tag{3.3}$$

$$n_\downarrow(t) = \frac{n}{2}[1-m(t)], \quad n_{B\downarrow}(t) = \frac{n_B}{2}[1-m_B(t)]. \tag{3.4}$$

Then (3.1) and (3.2) become linear:

$$\frac{d}{dt}m(t) = -\gamma n_B(m-m_B) \tag{3.5}$$

$$\frac{d}{dt}m_B(t) = \gamma n(m-m_B). \tag{3.6}$$

The solution is then

$$m(t) = \frac{1}{n+n_B}[B_0 + n_B A_0 e^{-\lambda t}] \tag{3.7}$$

$$m_B(t) = \frac{1}{n+n_B}[B_0 - n A_0 e^{-\lambda t}] \tag{3.8}$$

$$\lambda = \gamma(n+n_B), \tag{3.9}$$

where the constants $A_0 = m(0) - m_B(0), B_0 = nm + n_B m_B$ are set by the initial conditions.

As an example, assume that the bound electrons are initially unpolarized ($m_B(t=0) = 0$), while the conduction band electrons have an initial polarization of m_0. These initial conditions give $A_0 = m_0, B_0 = nm_0$.

$$m(t) = \frac{m_0}{n+n_B}[n + n_B e^{-\lambda t}] \tag{3.10}$$

$$m_B(t) = \frac{nm_0}{n+n_B}[1 - e^{-\lambda t}] \tag{3.11}$$

Note that, regardless of initial conditions, the two systems have the same fractional polarization for times $\lambda t >> 1$,

$$m(t=\infty) = m_B(t=\infty) = \frac{B_0}{n+n_B}. \tag{3.12}$$

Also, if $n >> n_B$, then the final fraction $m(\infty) \approx m_0 = m(0)$, and the spin polarization of the conduction electrons hardly changes. After the characteristic time $t_c = 1/\lambda$, the spin

system reaches a steady state with $m \approx m_B$, and no more spin depolarization occurs by this mechanism. Further spin relaxation can then occur by the spin-orbit channel described in Ref. [64].

As a simple model, consider a system with $n_B = 100$ bound electrons, which initially have $m_B(0) = 0, n_{B\uparrow} = n_{B\downarrow} = 50$. Inject a single spin-up electron into the conduction band. In time, it will exchange scatter and flip to the down position. Then there will be 51 bound electrons with spin up. The conduction electron, now with spin down, will scatter from one of these 51 down spins and go back to having spin up. The conduction electron spends slightly longer with the up spin arrangement, compared to the down spin arrangement, since there are 50 down spins to scatter from when it is up, but 51 up spins to scatter from when it is down. This makes the average polarization approximately 1%. The next two sections calculate the constant γ in two and three dimensions.

3.3 Three dimensions

The rate of spin exchange scattering is given by [72, 73]

$$\gamma = \frac{2\pi}{\hbar} \int \frac{d^3k_f}{(2\pi)^3} M^2 \delta(\varepsilon_i - \varepsilon_f) \tag{3.13}$$

with a matrix element of the form

$$M(\mathbf{k}_i, \mathbf{k}_f) = \frac{e^2}{\varepsilon_0} \int d^3r_1 d^3r_2 \phi_{1s}(r_1)\phi_{1s}(r_2) e^{i(\mathbf{k}_i\cdot\mathbf{r}_1 - \mathbf{k}_f\cdot\mathbf{r}_2)} \left[\frac{1}{r_1} - \frac{1}{r_{12}}\right] \tag{3.14}$$

$$\phi_{1s}(r) = \frac{1}{\sqrt{\pi a_0^3}} \exp(-r/a_0), \tag{3.15}$$

where a_0 is the effective Bohr radius of the donor in the effective mass approximation. In GaAs [74] it is around $a_0 = 10$ nm. We assume the scattering is elastic, so $k_f = k_i$; the integral (3.13), which is over all final states of the scattered electron, therefore becomes an angular integral only.

The two terms in (3.14) are evaluated separately:

$$M(\mathbf{k}_i, \mathbf{k}_f) = M_N(k) - M_x(\mathbf{k}_i, \mathbf{k}_f) \tag{3.16}$$

$$M_N(k) = \frac{32\pi e^2 a_0^2}{\varepsilon_0 (1+p^2)^3}, \quad p = ka_0. \tag{3.17}$$

In order to evaluate M_x, convert all variables to a dimensionless form: $\mathbf{p}_j = \mathbf{k}_j a_0, \vec{\rho}_j = \mathbf{r}_j/a_0$.

$$M_x = \frac{32\pi e^2 a_0^2}{\varepsilon_0} L(\mathbf{p}_i, \mathbf{p}_f) \tag{3.18}$$

$$L(\mathbf{p}_i, \mathbf{p}_f) = \frac{1}{32\pi^2} \int d^3\rho_1 d^3\rho_2 e^{-\rho_1-\rho_2} e^{i(\mathbf{p}_i\cdot\vec{\rho}_1 - \mathbf{p}_f\cdot\vec{\rho}_2)} \frac{1}{\rho_{12}} \tag{3.19}$$

At zero wave vector this produces

$$L(0,0) = \frac{5}{8}. \tag{3.20}$$

Note that the two terms in the matrix element do not cancel:

$$M(0,0) = \frac{12\pi e^2 a_0^2}{\varepsilon_0}. \tag{3.21}$$

The formulas for the scattering rate are now

$$\gamma(p) = 288\pi \frac{E_{Ry}}{\hbar}(a_0^3) I(p) \tag{3.22}$$

$$I(p) = \frac{64p}{9} \int \frac{d\Omega}{4\pi} \left[\frac{1}{(1+p^2)^3} - L(\mathbf{p}_i, \mathbf{p}_f) \right]^2, \tag{3.23}$$

where $d\Omega$ is the integral over 4π of solid angle. The large prefactor 288π comes from the factor of 12π in the matrix element. In GaAs [74], $E_{Ry} = 5.9$ meV. Then the numerical value of the prefactor is

$$\gamma_0 = 288\pi \frac{E_{Ry}}{\hbar} = 8.1 \times 10^{15} s^{-1}. \tag{3.24}$$

In order to estimate values of $p = ka_0$, consider the thermal energy, using the materials parameters of GaAs:

$$\frac{\hbar^2 k^2}{2m^*} = \frac{3}{2} k_B T, \;\; p^2 = 0.022T. \tag{3.25}$$

This gives p^2 =0.09 at $T = 4$K, and $p^2 = 1.7$ at $T = 77$K. At low temperature, p^2 is small and $L \approx 5/8$. At higher temperatures, the values of p^2 increase and L decreases.

One way to evaluate the integral is by Fourier transforming the Coulomb interaction,

which gives

$$L(p,\theta) = \frac{2}{\pi}\int_{-\infty}^{\infty} dq \int \frac{d\Omega}{4\pi} \frac{1}{[1+(\mathbf{p}_i+\mathbf{q})^2]^2[1+(\mathbf{p}_f+\mathbf{q})^2]^2}. \tag{3.26}$$

Write the denominator as

$$L(p,\theta) = \frac{2}{\pi}\int_{-\infty}^{\infty} dq \int \frac{d\Omega}{4\pi} \frac{1}{[(q+q_i)^2+a_i^2]^2[(q+q_f)^2+a_f^2]^2} \tag{3.27}$$

$$q_j = p\nu_j, \quad a_j^2 = 1+p^2(1-\nu_j^2) \tag{3.28}$$

$$\nu_i = \hat{p}_i\cdot\hat{q}, \quad \nu_f = \hat{p}_f\cdot\hat{q}, \quad \cos(\theta) = \hat{p}_i\cdot\hat{p}_f. \tag{3.29}$$

The integral over dq can be evaluated by contour integration:

$$L(p,\theta) = \int \frac{d\Omega}{4\pi}\frac{1}{a_i^2 a_f^2 D^2}\left[\frac{a_i^3+a_f^3}{a_i a_f} + \frac{4(a_i+a_f)^3}{D}\right] \tag{3.30}$$

$$D = (a_i+a_f)^2 + (q_i-q_f)^2. \tag{3.31}$$

For forward scattering one finds that

$$L(p,0) = \frac{1}{8}\left[\frac{1}{1+p^2} + \frac{4/3}{(1+p^2)^2} + \frac{8/3}{(1+p^2)^3}\right]. \tag{3.32}$$

For back scattering, $\nu_f = -\nu_i, D = 4(1+p^2)$, and

$$L(p,\pi) = \frac{1}{8(1+p^2)^3}\left[1+\frac{4}{p}\sin^{-1}\left(\frac{p}{\sqrt{1+p^2}}\right)\right]. \tag{3.33}$$

By comparing (3.32) and (3.33), one sees that $L(p,\theta)$ is largest at $\theta = 0$ and decreases with increasing angle.

For a general scattering angle θ one can compute (3.30) numerically. Another method for evaluating the integral is to write it as

$$L(p,\theta) = \sum_{n=0} b_n(p) P_n(\theta) \tag{3.34}$$

$$b_0 = \frac{5+p^2}{8(1+p^2)^3}. \tag{3.35}$$

The other b_n are much smaller, so an adequate approximation to the cross section in three dimensions is to set $L \approx b_0$ and get isotropic scattering

$$I(p) = \frac{p(3-p^2)^2}{3^2(1+p^2)^6}, \tag{3.36}$$

where $p = ka_0$. Since $I(0) = 0$, the maximum value of this function is at $p = 0.283$ where $I \approx 1/6$. That is the value of $p^2 = 0.08$ corresponding to the thermal energy at $T = 4$K.

3.4 Two dimensions

The electron scattering rate in two dimensions is given by

$$\gamma = \frac{2\pi}{\hbar} \int \frac{d^2k_f}{(2\pi)^2} M^2 \delta(\varepsilon_i - \varepsilon_f). \tag{3.37}$$

The matrix element for exchange scattering has the form

$$M(\mathbf{k}_i, \mathbf{k}_f) = \frac{e^2}{\varepsilon_0} \int d^2r_1 d^2r_2 \phi_{1s}(r_1)\phi_{1s}(r_2) e^{i(\mathbf{k}_i\cdot\mathbf{r}_1 - \mathbf{k}_f\cdot\mathbf{r}_2)} \left[\frac{1}{r_1} - \frac{1}{r_{12}}\right] \tag{3.38}$$

$$\phi_{1s}(r) = \frac{\sqrt{8}}{\sqrt{\pi}a_0} \exp(-2r/a_0), \tag{3.39}$$

where a_0 is the effective Bohr radius of the donor in three dimensions. We assume the scattering to be elastic, so $k_f = k_i$ and they differ only in their angle. We define zero angle as the direction of $\mathbf{k}_i$, so that the direction of $\mathbf{k}_f$ is the scattering angle θ. The matrix element has two terms, and the first one is a straightforward integral. Define $p = ka_0/2$:

$$M_N(p) = \frac{4\pi e^2 a_0}{\varepsilon_0 (1+p^2)^2}. \tag{3.40}$$

In order to evaluate M_x, convert all variables to a dimensionless form: $\mathbf{p}_j = \mathbf{k}_j a_0/2, \vec{\rho}_j = 2\mathbf{r}_j/a_0$.

$$M_x = \frac{4\pi e^2 a_0}{\varepsilon_0} L(p,\theta) \tag{3.41}$$

$$L(p,\theta) = \frac{1}{4\pi^2} \int d^2\rho_1 d^2\rho_2 e^{-\rho_1-\rho_2} e^{i(\mathbf{p}_i\cdot\vec{\rho}_1 - \mathbf{p}_f\cdot\vec{\rho}_2)} \frac{1}{\rho_{12}} \tag{3.42}$$

The integral L is evaluated in Fourier transform space. Taking the two-dimensional transform of the Coulomb potential, we put the integral in the dimensionless form

$$L(y,\theta) = \int_0^\infty dx \int_0^{2\pi} \frac{d\phi}{2\pi} G(x,y,\phi)G(x,y,\theta-\phi) \tag{3.43}$$

$$G(x,y,\phi) = \frac{1}{[1+x^2+y^2+2xy\cos(\phi)]^{3/2}} \tag{3.44}$$

$(x = qa_0/2, y = ka_0/2)$. This integral is hard to evaluate. It can be done for a few special cases. The first is setting $k = 0$ $(y = 0)$.

$$L(0,0) = \int_0^\infty \frac{dx}{[1+x^2]^3} = \frac{3\pi}{16} \tag{3.45}$$

Note that this is not equal to $M_N(0)$, and again the two terms do not cancel at forward scattering. The exchange scattering constants are

$$\gamma(y) = 32\pi^2 \frac{E_{Ry}}{\hbar}(a_0^2)I(y) \tag{3.46}$$

$$I(y) = \int_0^{2\pi} \frac{d\theta}{2\pi}\left[\frac{1}{(1+y^2)^2} - L(y,\theta)\right]^2, \tag{3.47}$$

where E_{Ry} is the binding energy of a three-dimensional donor. The prefactor of the above expression is

$$32\pi^2 \frac{E_{Ry}}{\hbar} = 2.8 \times 10^{15} s^{-1}. \tag{3.48}$$

$L(y,\theta)$ may be evaluated by performing a Fourier expansion in the angle, and retaining only a few terms,

$$L(y,\theta) = \sum_{n=0} a_n(y)\cos(n\theta). \tag{3.49}$$

It is useful to define

$$J_n(x,y) = \int_0^{2\pi} \frac{d\phi}{2\pi} \frac{\cos(n\phi)}{[1+x^2+y^2+2xy\cos(\phi)]^{3/2}} \tag{3.50}$$

$$a_n(y) = \varepsilon_n \int_0^\infty dx J_n(x,y)^2 \tag{3.51}$$

$$\varepsilon_0 \;=\; 1,\;\; \varepsilon_n = 2,\;\; n \geq 1. \tag{3.52}$$

The J_n can be expressed in terms of elliptic integrals. Let $\phi = 2\alpha$ and

$$J_n(x,y) \;=\; \frac{2/\pi}{[1+(x+y)^2]^{3/2}} \int_0^{\pi/2} \frac{d\alpha \cos(2n\alpha)}{[1-m\cos^2(\alpha)]^{3/2}} \tag{3.53}$$

$$m \;=\; \frac{4xy}{1+(x+y)^2} \leq 1 \tag{3.54}$$

$$a_n(0) \;=\; \frac{3\pi}{16}\delta_{n=0}. \tag{3.55}$$

At small values of y, then, $a_n(y) \sim y^n$. The lowest few functions are

$$J_0 \;=\; \frac{2/\pi}{[1+(x+y)^2]^{3/2}}[K + 2m\frac{dK}{dm}] \tag{3.56}$$

$$J_1 \;=\; \frac{2/\pi}{[1+(x+y)^2]^{3/2}}[2(2-m)\frac{dK}{dm} - K] \tag{3.57}$$

$$J_2 \;=\; \frac{2/\pi}{m^2[1+(x+y)^2]^{3/2}}\left[8(E-K) + m^2K + 2m\frac{dK}{dm}(8-8m+m^2)\right]$$

$$K(m) \;=\; \int_0^{\pi/2} \frac{d\alpha}{\sqrt{1-m\cos^2(\alpha)}},\;\; E(m) = \int_0^{\pi/2} d\alpha\sqrt{1-m\cos^2(\alpha)}. \tag{3.58}$$

We have evaluated these expressions, and find, as in three dimensions, that an accurate approximation for the wave vector dependence need retain only the first term in the series,

$$I(y) \;\approx\; \left[\frac{1}{(1+y^2)^2} - a_0(y)\right]^2. \tag{3.59}$$

In two dimensions, the function $\gamma(y)$ has its largest value at $y = 0$, and decreases for increasing values of $y = ka_0/2$.

3.5 Discussion

We have shown that spin exchange scattering defines a rate constant γ. Using this rate constant, we derived and solved a set of rate equations which determine the final degree of spin polarization of the conduction band. This seems to be a fast process, so that the final degree of spin polarization is reached rapidly.

One straightforward application of our result is to compare the mean scattering time to

the conventional D'yakonov-Perel' scattering time. Because the latter is a property of the crystal, not its impurities, this outcome will vary from sample to sample. The nonrelativistic effect can probably be disregarded in a single-junction GaAs device, whose D'yakonov-Perel' coupling is known to be unusually large [75, 76]. In other cases, however, either phenomenon could be the dominant empirical consideration (when performing a curve fit to low-energy photoluminescence data, for example), and both rate constants should be evaluated, assuming that the concentration of neutral impurities in a given sample can be estimated.

The spin exchange scattering is affected by the density n_B of scattering centers; the spin polarization lifetime

$$\frac{1}{\tau} = \gamma(n + n_B) \tag{3.60}$$

depends upon this density. This number will vary from sample to sample, and become very small in nominally pure samples. All semiconductors have some impurities. Some may be shallow donors, while others have a larger binding energy. Since these defects can trap electrons, they serve as scattering sites that can exchange scatter with the band electron. In three dimensions, at high doping, if one is above the Mott limit ($n_D^{1/3} a_0 > 0.24$), the average binding energy of the donors goes to zero. Then n_B will be very small. Due to the random locations of the donors, some will still be clustered and lead to bound electrons. These are the donors that give rise to the well-known band tails. In many pump-probe optical experiments, a temporary density of excitons is created, which could also exchange scatter a band electron.

In two dimensions, the binding energy does not vanish at any electron density, so there are always electrons bound to donors. Many experiments are done in quantum wells or superlattices. These states are midway between two and three dimensions: they are three-dimensional, but the confinement to the quantum well makes them quasi-two-dimensional. In this case the location of the donor is important for the calculation of the cross section: whether it is in the quantum well, or outside in the barrier layer.

Chapter 4

Role of diffusion in the operation of semiconductor microdisk lasers

4.1 Introduction

The experimental field of quantum well lasers is large and continues to expand [58, 77]. However, a general theoretical approach incorporating dissipative effects is still a subject of some debate [56, 78, 79, 80]. Many forms of noise and decoherence are routinely used as qualitative explanations of experimental results, but omitted from microscopic models due to perceived mathematical intractability. Examples include local heating at high pump energies [61, 81], interface roughness in heterostructures [82], and spin depolarization by surface phonons [83].

Our present goal is a numerical simulation of charge diffusion of conduction electrons in a semiconductor laser. Previous analyses have usually neglected diffusion on the grounds that its characteristic time scale is much shorter than a single lasing cycle [3, 84, 85, 86]. In microcavity lasers, where electron lifetimes are greatly enhanced due to photon coupling [87], this assumption must be reevaluated. The spatial distribution of electrons is especially significant in a microdisk because non-radiative recombination at the disk edges is a primary cause of energy loss [88]; on the other hand, electromagnetic modes in cavities are known to be spatially nonuniform [89], so a nonuniform electron distribution may actually enhance electron-photon coupling. Other studies have incorporated diffusion in a phenomenological way, without adding it to the electron Hamiltonian [90, 91, 92].

Our system is a semiconductor microdisk with several quantum wells separated by buffer

layers. The band edges at $k = 0$ are farther apart in the buffers, so any electron-hole pair created in a buffer quickly migrates into a well [13]. The wells therefore form the active regions of the laser. A single optical cavity mode, with an energy near the gap energy, can be populated by pair recombination and thereby contribute to stimulated emission [93]. We wish to compute the time evolution of the electron and photon concentrations between two consecutive pump pulses, with and without diffusion.

4.2 Rate equations

A direct-gap semiconductor coupled to cavity photons is described by the optical Bloch equations [94]. In general, the dependent variables include an occupation number for each accessible k in the upper band, which can easily contain 10^4 electrons even in a disk several microns across [95]. However, many workers have noted that the measured photoemissions vary on a time scale of order 20 ps, which is long compared to the thermal relaxation time of the conduction electrons [63, 96]. It is therefore reasonable to assume a Fermi sea, where intraband transitions can be neglected. One averages the basic equations over k and spin, obtaining a single differential equation per particle species.

We base our calculation closely on that of Luo et al., which successfully matched the results of a particular experiment [62], yet has sufficiently general features to apply to a wide class of semiconductor lasers. That analysis assumed a three-dimensional active region. In the remainder of this section we modify it to describe two-dimensional quantum wells.

The total microdisk height is comparable to the optical wavelengths in the system. Therefore, materials constants involving the lattice ions can be adapted by simple dimensional analysis [97]. The same is not true of charge screening within the conduction band: each electron is spatially confined, but its Coulomb field remains three-dimensional. We use a modified Thomas-Fermi approach [98] which also accounts for scattering by impurities in the buffer layers; the matrix element in frequency space is

$$\tilde{V}(q) = \frac{e^2}{2\epsilon_0\epsilon_r}\frac{\exp(-qd)}{q + q_{TF}G(q)} \tag{4.1}$$

$$q_{TF} = \frac{m_e e^2}{2\pi\epsilon_0\epsilon_r\hbar^2} \tag{4.2}$$

$$G(q) = \frac{1}{8}\left[2\left(\frac{b}{b+q}\right)^3 + 3\left(\frac{b}{b+q}\right)^2 + 3\left(\frac{b}{b+q}\right)\right] \tag{4.3}$$

$$b = \left(\frac{33 m_e e^2 n}{8\hbar^2 \epsilon_0 \epsilon_r}\right)^{1/3} \tag{4.4}$$

with $\epsilon_r = 13.1$ and $d \approx 45$nm, the mean electron-electron distance.

Instead of a time-varying injection term, we postulate a spatially uniform initial population of electrons. This avoids the non-trivial issue of choosing a numeric time step for a system of equations with two very disparate characteristic time scales [99]; consequently a far wider range of concentrations may be safely analyzed. Mathematically, this also prevents us from using the pump pulse width as a fit parameter as in Ref. [62]; we must add an explicit diffusion term also.

We compute $N(t = 0)$ as a function of energy using a parabolic density of states in two dimensions [100]. Using the experimental parameters of Ref. [62] we find that, even at high pump powers, less than 10 percent of the conduction band is filled. This supports our use of the Thomas-Fermi function. Very large inversions [101] require a true many-body treatment such as Hartree-Fock. Pair recombination is suppressed by rapid spin dephasing in the hole bands [102], so the initial quasi-Fermi level follows directly from energy conservation and a spin selection rule.

We thus arrive at the following rate equations for the electron and photon concentrations:

$$\frac{\partial}{\partial t} n(\mathbf{r}, t) = -\frac{1}{\tau_C} n - \Gamma s G_0 (n - n_0) - B n^2 + D \nabla^2 n \tag{4.5}$$

$$\frac{\partial}{\partial t} s(\mathbf{r}, t) = -\frac{1}{\tau_p} s + \Gamma s G_0 (n - n_0) + \beta B n^2 \tag{4.6}$$

with τ_C =500 ps, $\tau_p = 5$ ps, $\Gamma = 0.45$, $\beta = 0.01$, $B = 1.25 \times 10^{-4}$ cm^2/s, $G_0 = 2.5$ cm^2/s, and $n_0 = 2.32 \times 10^{12}$ cm^{-2} (the transparency point). The linear terms represent spontaneous emission, the n^2 terms represent emission into the cavity mode, and the cross terms represent stimulated emission. The diffusion constant is found using $D = \bar{v}^2 \tau / 2$, where τ corresponds to the mobility and $\bar{v}$ is the average velocity.

4.3 Simulations

We discretize our equations using a conventional scheme with forward time derivatives and centered spatial derivatives. No formal method exists for the stability analysis of nonlinearly coupled equations [103, 104, 105], so we perform a heuristic check. Each equation is made

dimensionless by choosing characteristic length and time scales such that each constant coefficient is of order 1 or lower (and preferably of order 0.1 or lower). We then vary the spatial and temporal grid sizes to test whether small changes produce qualitatively different particle counts. No such chaotic behavior is observed, although some roundoff error appears at extremely small mesh sizes (far smaller than are used in the graphs below).

In the absence of applied EM fields, each quantum well has azimuthal symmetry. Only the radial coordinate is non-trivial. Boundary conditions are set by assuming zero concentration outside the disk, and a smooth gradient at the center. It is generally believed that the optical cavity modes are highly localized near the disk edge [106]; the coupling β is therefore weighted to be zero everywhere except in the outermost annulus, while still averaging to 0.01.

The experimental signature of a lasing threshold is a local minimum in delay time versus pump power [107, 108]. We successfully reproduced this with $D = 0$ (Fig. 4.1). In the presence of diffusion, the delay time decreases at all pump powers, but a qualitative change requires a physically large diffusion effect. For example, a term with $D = 100$ cm^2/s shifts the delay time at threshold by about 15 percent (Fig. 4.2). This corresponds to an electron mobility of 1.5×10^4 cm^2/V s at 77 K.

4.4 Discussion

Using two coupled rate equations with an explicit diffusion term, we have reproduced the essential features of the photoemission data reported in Ref. [62]. Our formalism contains no adjustable constants specific to that experiment; it should apply to any similar semiconductor microdisk.

At extremely large values of D, the lasing threshold itself increases (Fig. 4.3). This prediction is sensible, since faster diffusion would increase non-radiative recombination at the disk edge, reducing pump efficiency. In the next few years, it should be possible to fabricate heterostructures with such high mobilities [109].

In our dimensionless rate equations, the spontaneous emission term clearly dominates for any physically reasonable value of D. This could suggest that a uniformly fabricated disk is inherently limited in its coupling to optical modes. Some experiments deliberately introduce irregularities into their heterostructures [60, 110] to increase photon count. Systematic engineering of such defects would be greatly aided by a more detailed microscopic model. This

is a subject for future theoretical research.

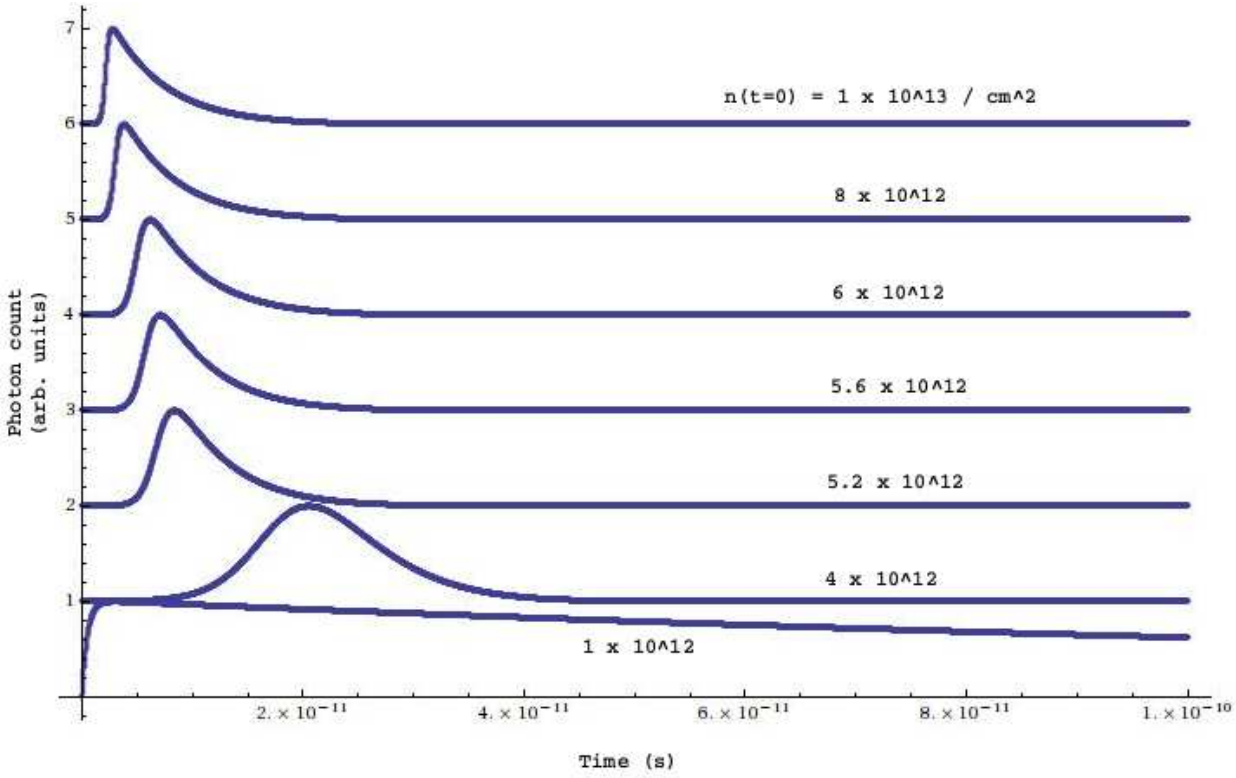

Figure 4.1. Time-resolved photon concentrations (normalized and offset for clarity) for a microdisk quantum well laser without diffusion. As the pump power increases, we see a local minimum in the delay time (i.e. between pump pulse and peak emission), which signifies a lasing threshold. Using the pump energies of Ref. [62], we obtain a maximum electron concentration around $10^{12}/\text{cm}^2$, which is within typical experimental bounds [101]. The simulation uses 10 radial mesh points and a time step of 20 fs.

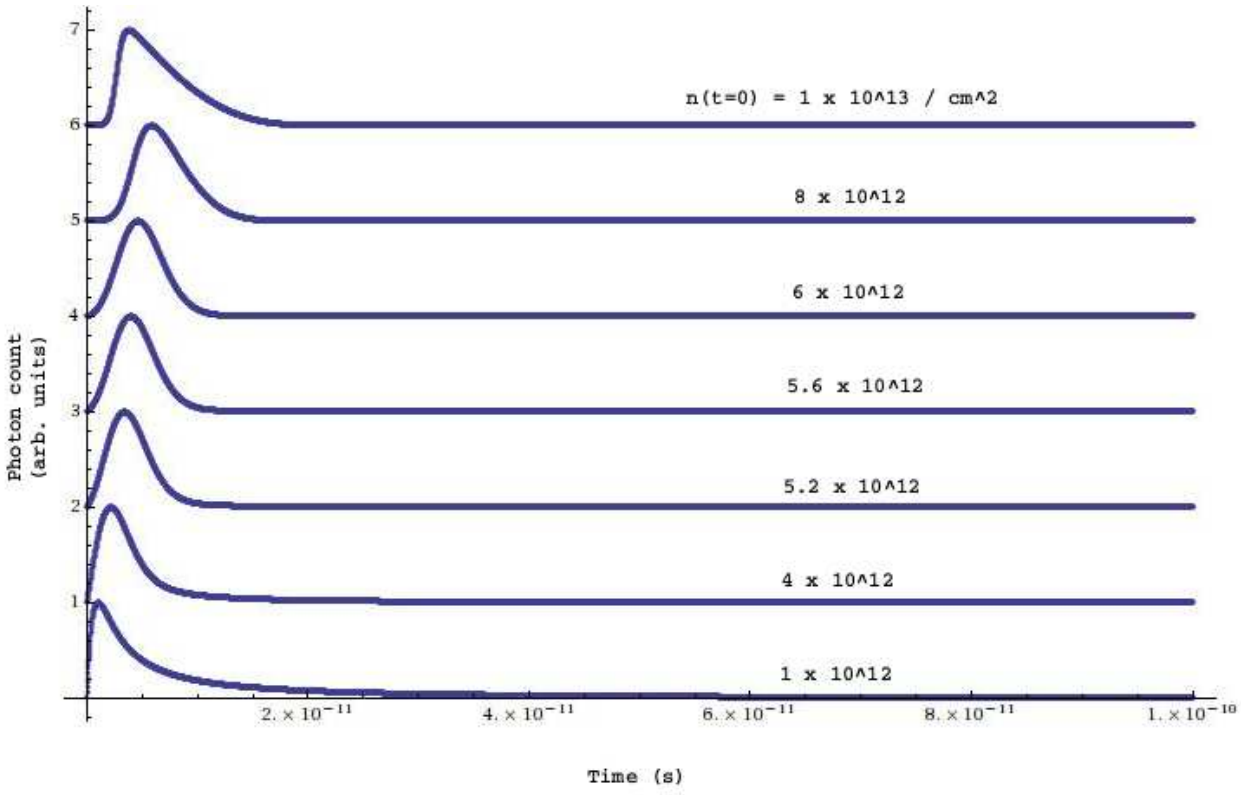

Figure 4.2. Time-resolved photon concentrations (normalized and offset for clarity) for a microdisk quantum well laser with $D = 100$ cm^2/s in the conduction band. With the addition of a significant diffusion mechanism, the delay time is roughly halved, because the optical cavity mode (localized near the disk edge) can be populated more efficiently. The simulation uses 10 radial mesh points and a time step of 20 fs.

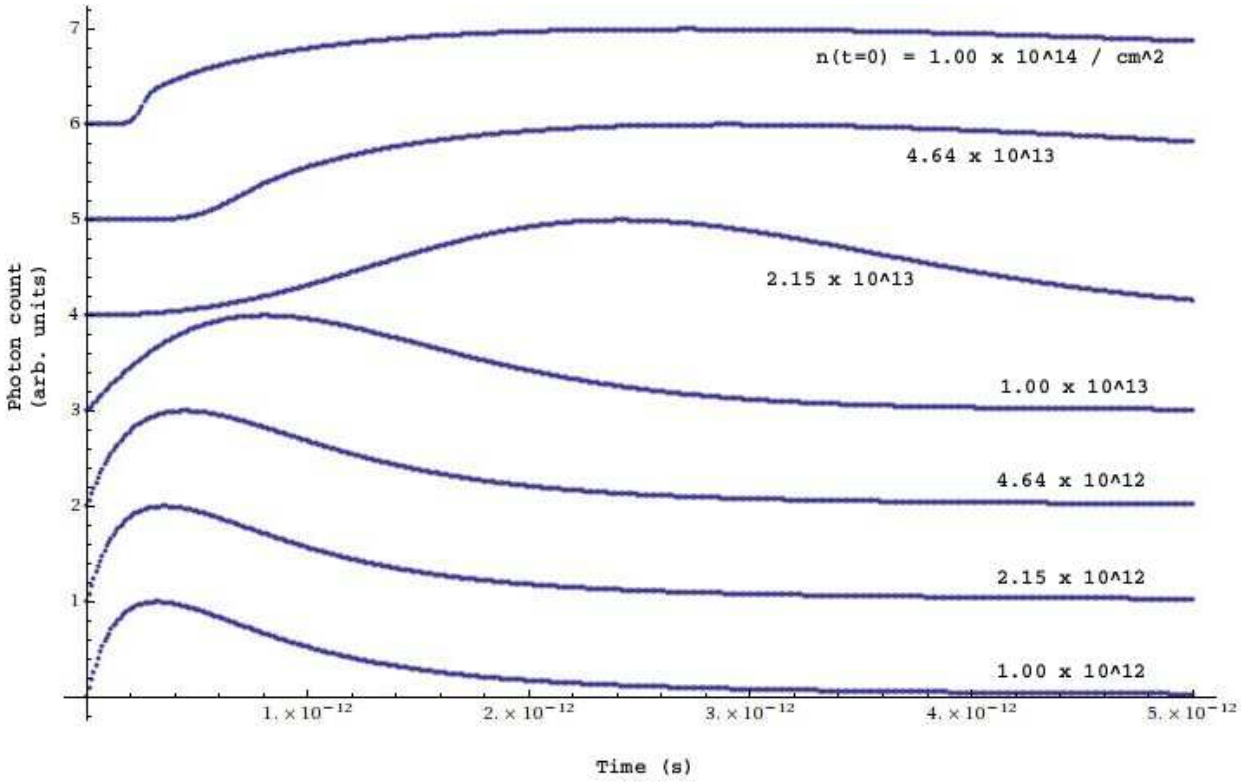

Figure 4.3. Time-resolved photon concentrations (normalized and offset for clarity) for a microdisk quantum well laser with $D = 2000$ cm^2/s in the conduction band. A huge diffusion effect causes the lasing threshold to increase significantly (note the greater range of pump powers); the reasons for this are unclear, but probably the conduction electrons are being rapidly "drained" by the boundary condition of zero concentration at the outer edge. The simulation uses 10 radial mesh points and a time step of 10 fs.

Appendix

Derivation of constraints on four-body coupling terms for encoded qubits

A.1 The U_A Gate

U_A only involves a single exchange interaction and so is unmodified in the presence of the three- and four-body corrections:

$$
\begin{aligned}
U'_A &= U_A = \exp\left[-\frac{i}{2}\cos^{-1}(-1/3)E_{DE}\right] \\
&= \begin{pmatrix}
\alpha & & & & \frac{1}{i\sqrt{2}} & & & & & & & & & & & \\
& \alpha & & & & & \frac{1}{i\sqrt{2}} & & & & & & & & & \\
& & \alpha & & & \frac{1}{i\sqrt{2}} & & & & & & & & & & \\
& & & \alpha & & & & \frac{1}{i\sqrt{2}} & & & & & & & & \\
\frac{1}{i\sqrt{2}} & & & & \alpha^* & & & & & & & & & & & \\
& & \frac{1}{i\sqrt{2}} & & & \alpha^* & & & & & & & & & & \\
& \frac{1}{i\sqrt{2}} & & & & & \alpha^* & & & & & & & & & \\
& & & \frac{1}{i\sqrt{2}} & & & & \alpha^* & & & & & & & & \\
& & & & & & & & \beta & & & & & & & \\
& & & & & & & & & \beta & & & & & & \\
& & & & & & & & & & \frac{1}{\sqrt{3}}+\frac{1}{2i\sqrt{6}} & \frac{1}{2i}\sqrt{\frac{5}{2}} & & & & \\
& & & & & & & & & & \frac{1}{2i}\sqrt{\frac{5}{2}} & \frac{1}{\sqrt{3}}-\frac{1}{2i\sqrt{6}} & & & & \\
& & & & & & & & & & & & \beta & & & \\
& & & & & & & & & & & & & \beta & &
\end{pmatrix},
\end{aligned}
$$

where $\alpha = \frac{\sqrt{2}-i}{\sqrt{6}}$ and $\beta = e^{-i/[2\cos^{-1}(-3)]}$.

A.2 The U_5 Gate

U_5 involves dots F, G, and H, with dots F and H simultaneously coupled to G, and hence experiences a three-body correction to the exchange constants. In addition, a coupling between dot F and dot H will arise which forces our modified U_5 gate to have the form

$$
\begin{aligned}
U_5' &= \exp\left[\frac{i\pi}{\sqrt{3}}\left(E_{FG} + \frac{1}{2}E_{GH} + J_5' E_{FH}\right)\right] \\
&= \begin{pmatrix}
p & \Phi & & & & & & & & & & & & & & \\
\Phi & p^* & & & & & & & & & & & & & & \\
 & & p & \Phi & & & & & & & & & & & & \\
 & & \Phi & p^* & & & & & & & & & & & & \\
 & & & & p & & \Phi & & & & & & & & & \\
 & & & & & p & & \Phi & & & & & & & & \\
 & & & & \Phi & & p^* & & & & & & & & & \\
 & & & & & \Phi & & p^* & & & & & & & & \\
 & & & & & & & & e^{\frac{i\pi(2J_5'+3)}{2\sqrt{3}}} & & & & & & & \\
 & & & & & & & & & p & & & & & \Phi & \\
 & & & & & & & & & & e^{\frac{i\pi(2J_5'+3)}{2\sqrt{3}}} & & & & & \\
 & & & & & & & & & & & e^{\frac{i\pi(2J_5'+3)}{2\sqrt{3}}} & & & & \\
 & & & & & & & & & & & & e^{\frac{i\pi(2J_5'+3)}{2\sqrt{3}}} & & & \\
 & & & & & & & & & \Phi & & & & & p^* &
\end{pmatrix},
\end{aligned}
$$

where

$$
\begin{aligned}
\Lambda &= \sqrt{\tfrac{4}{3}(J_5')^2 - 2J_5' + 1} \\
p &= \cos\left[\frac{\pi}{2}\Lambda\right] + \frac{iJ_5'}{\sqrt{3}\Lambda}\sin\left[\frac{\pi}{2}\Lambda\right] \\
\Phi &= \frac{i}{J_5'}(1 - J_5')\sin\left[\frac{\pi}{2}\Lambda\right].
\end{aligned}
$$

It is seen that this gate operates "classically", and is non-diagonal, only when J_5' is either 0 or chosen such that Λ is an even integer. In both cases we recover Bacon's functional form:

$$U_5 = \begin{pmatrix}
 & i & & & & & & & & & & & & & & & \\
i & & & & & & & & & & & & & & & & \\
 & & & i & & & & & & & & & & & & & \\
 & & i & & & & & & & & & & & & & & \\
 & & & & & i & & & & & & & & & & & \\
 & & & & & & i & & & & & & & & & & \\
 & & & & i & & & & & & & & & & & & \\
 & & & & & i & & & & & & & & & & & \\
 & & & & & & & e^{i\frac{\sqrt{3}\pi}{2}} & & & & & & & & & \\
 & & & & & & & & & & & & & & & i & \\
 & & & & & & & & & e^{i\frac{\sqrt{3}\pi}{2}} & & & & & & & \\
 & & & & & & & & & & & e^{i\frac{\sqrt{3}\pi}{2}} & & & & & \\
 & & & & & & & & & & & & & e^{i\frac{\sqrt{3}\pi}{2}} & & & \\
 & & & & & & & & & & i & & & & & & \\
\end{pmatrix}.$$

A.3 The U_B Gate

Bacon's U_B gate is

$$\begin{aligned} U_B &= \exp\left[-\frac{i\pi}{2}\left(\sum_{A=i<j}^{D} E_{ij}\right)\right] \\ &= \mathrm{diag}(1,1,1,1,-1,-1,-1,-1,-1,-1,-1,-1,-1,-1). \end{aligned}$$

U_B involves coupling between four dots and so experiences both quantitative three-body corrections and a four-body qualitative correction. Since the four spins in U_B are coupled symmetrically, the form of the four-body correction must also be symmetric:

$$\begin{aligned} U'_B &= \exp\{-\frac{i\pi}{2}[\sum_{A=i<j}^{D} E_{ij} + J'_B(E_{AB}E_{CD} + E_{AC}E_{BD} + E_{AD}E_{BC})]\} \\ &= \mathrm{diag}(\gamma^{-3},\gamma^{-3},\gamma^{-3},\gamma^{-3},-\gamma,-\gamma,-\gamma, \\ &\quad -\gamma,-\gamma,-\gamma,-\gamma,-\gamma^{-3},-\gamma,-\gamma), \end{aligned}$$

where $\gamma = e^{\frac{i\pi}{2}J'_B}$. Note that because U'_B forms part of the U'_6 gate, which acts on $S_{\mathrm{T}} = 0$ states outside of the code space, the action of the four-body terms in it is non-trivial for

arbitrary J_B'. However, upon setting J_B' to any integer value, we recover U_B up to an overall phase.

A.4 The U_2, U_3 Gates

U_2 and U_3 similarly involve coupling between four dots inside a fixed code block, and so also experience both quantitative three-body corrections and a four-body qualitative correction. In this case the Heisenberg couplings are not symmetric, so we do not assume that all four-body terms are turned on with equal coupling constants:

$$\begin{aligned} U_2' &= \exp\{\frac{i\pi}{4\sqrt{2}}[-3E_{EF} - \frac{2}{3}(E_{FG} + E_{FH} + E_{GH}) \\ &\quad + J_2' E_{EF}E_{GH} + J_2''(E_{AC}E_{BD} + E_{EH}E_{FG})]\} \\ &= \begin{pmatrix} \delta & & & & & & & & & & & & & & & \\ & \epsilon & & & & & & & & & & & & & & \\ & & \delta & & & & & & & & & & & & & \\ & & & \epsilon & & & & & & & & & & & & \\ & & & & \zeta & & & & & & & & & & & \\ & & & & & \zeta & & & & & & & & & & \\ & & & & & & \eta & & \rho & & & & & & & \\ & & & & & & & \eta & & & & & & \rho & & \\ & & & & & & \rho & & \eta^* & & & & & & & \\ & & & & & & & & & \zeta & & & & & & \\ & & & & & & & & & & \eta^* & & & & & \rho \\ & & & & & & & & & & & e^{i\pi\frac{(-5+J_2'+2J_2'')}{4\sqrt{2}}} & & & & \\ & & & & & & & \rho & & & & & & \eta^* & & \\ & & & & & & & & & & \rho & & & & & \eta \end{pmatrix} \end{aligned}$$

and

$$\begin{aligned} U_3' &= \exp\{\frac{i\pi}{4\sqrt{2}}[-3E_{CD} - \frac{2}{3}(E_{AB} + E_{AC} + E_{BC}) \\ &\quad + J_3' E_{AB}E_{CD} + J_3''(E_{AC}E_{BD} + E_{AD}E_{BC})]\} \end{aligned}$$

$$= \begin{pmatrix}
\delta & & & & & & & & & & & & & & & \\
& \delta & & & & & & & & & & & & & & \\
& & \epsilon & & & & & & & & & & & & & \\
& & & \epsilon & & & & & & & & & & & & \\
& & & & \zeta & & & & & & & & & & & \\
& & & & & \eta & & & \rho & & & & & & & \\
& & & & & & \zeta & & & & & & & & & \\
& & & & & & & \eta & & & & & & & \rho & \\
& & & & & & & & \zeta & & & & & & & \\
& & & & & \rho & & & \eta^* & & & & & & & \\
& & & & & & & & & \eta^* & & & & \rho & & \\
& & & & & & & & & & e^{i\pi\frac{(-5+J_3'+2J_3'')}{4\sqrt{2}}} & & & & & \\
& & & & & & & & & \rho & & & & \eta & & \\
& & & & & & \rho & & & & & & & & \eta^* &
\end{pmatrix},$$

where

$$\begin{aligned}
\nu &= \sqrt{3(J_k')^2 + 3(J_k'')^2 - 6J_k'J_k'' - 16J_k' + 16J_k'' + 24} \\
\delta &= e^{i\pi\frac{1}{4\sqrt{2}}\left(J_k'+2J_k''+3\right)} \\
\epsilon &= e^{i\pi\frac{1}{4\sqrt{2}}\left(J_k'+2J_k''+3\right)} \\
\zeta &= e^{-i\pi\frac{1}{4\sqrt{2}}\left(J_k'+3\right)} \\
\eta &= e^{-i\pi\frac{1}{4\sqrt{2}}}\left[\cos\left(\frac{\pi\nu}{4\sqrt{6}}\right) - \frac{1}{\sqrt{3}\nu}(J_k' - J_k'')\sin\left(\frac{\pi\nu}{4\sqrt{6}}\right)\right] \\
\rho &= \frac{\sqrt{2}(3 - J_k' + J_k'')}{\sqrt{3}\nu} e^{-\frac{i\pi}{4\sqrt{2}}\left[1+J_k''-\frac{\nu}{\sqrt{3}}\right]}\left[1 - e^{\frac{i\pi\nu}{2\sqrt{6}}}\right]
\end{aligned}$$

and $k = 2$ (3) for U_2' (U_3'). It turns out that these two gates can act "classically" only when $\eta = 0$, which produces a transcendental equation relating J_k' and J_k'' ($J_k' = J_k''$ is one class of solutions).

A.5 The U_1 Gate

The U_1 gate is qualitatively different from all the previous gates: it involves an interaction among five dots and between two code blocks. In this case the effect of the four-body

interactions is generally to strongly interfere with the action of U_1. Therefore we must carefully re-examine this gate and consider whether it can be made compatible with the four-body effect. The generator of U_1 is

$$H_1 = E_{DE} + \frac{1}{2}\sum_{A=i<j}^{D} E_{ij},$$

and the modified generator, in the presence of four-body interactions, is in general

$$H_1' = H_1 + \sum_{A=i<j<k<l}^{E} J'_{ij;kl} E_{ij} E_{kl}.$$

Therefore the new gate will have the form

$$U_1' = \exp(\frac{i\pi}{\sqrt{3}} H_1').$$

There are symmetry relations between the constants $J'_{ij;kl}$: the magnitudes of the exchange interactions in H_1 imply an equivalence between spins A, B, and C, while spins D and E are distinct. Thus there will be four such constants, corresponding to the following sets of inequivalent two-body pairings:

- one of spins $\{A, B, C\}$ coupled with spin D but not with spin E: $J'_a \equiv J'_{AB;CD} = J'_{AC;BD} = J'_{BC;AD}$;
- one of spins $\{A, B, C\}$ coupled with spin E but not with spin D: $J'_b \equiv J'_{AB;CE} = J'_{AC;BE} = J'_{BC;AE}$;
- spin D coupled with spin E: $J'_c \equiv J'_{AB;DE} = J'_{AC;DE} = J'_{BC;DE}$;
- one of spins $\{A, B, C\}$ coupled with spin D, one with spin E: $J'_d \equiv J'_{AD;BE} = J'_{AD;CE} = J'_{BD;AE} = J'_{BD;CE} = J'_{CD;AE} = J'_{CD;BE}$.

Thus U_1' can be written as

$$\begin{aligned} U_1' \;=\; & \exp\{\frac{i\pi}{\sqrt{3}}[E_{DE} + \frac{1}{2}\sum_{A=i<j}^{D} E_{ij} + J'_a(E_{AB}E_{CD} + E_{AC}E_{BD} + E_{AD}E_{BC}) \\ & + J'_b(E_{AB}E_{CE} + E_{AC}E_{BE} + E_{AE}E_{BC}) \end{aligned}$$

$$
\begin{aligned}
&+J'_c(E_{AB}E_{DE}+E_{AC}E_{DE}+E_{BC}E_{DE})\\
&+J'_d(E_{AD}E_{BE}+E_{AD}E_{CE}+E_{AE}E_{BD}\\
&\quad +E_{AE}E_{CD}+E_{BD}E_{CE}+E_{BE}E_{CD})]\}
\end{aligned}
\tag{A.1}
$$

$$
= \begin{pmatrix}
\chi_+ & & & \lambda & & & & & & & & \\
& \chi_+ & & & \lambda & & & & & & & \\
& & \chi_+ & & & \lambda & & & & & & \\
& & & \chi_+ & & & \lambda & & & & & \\
\lambda & & & & \chi_- & & & & & & & \\
& \lambda & & & & \chi_- & & & & & & \\
& & \lambda & & & & \chi_- & & & & & \\
& & & \lambda & & & & \chi_- & & & & \\
& & & & & & & & \xi & & & \\
& & & & & & & & & \theta & & \\
& & & & & & & & & & \tau_- & \mu \\
& & & & & & & & & & \mu & \tau_+ \\
& & & & & & & & & & & & \xi & \\
& & & & & & & & & & & & & \theta
\end{pmatrix},
$$

where

$$
\begin{aligned}
x &= \left\{9\left(1+4J'_b-4J'_d\right)+48\left[{J'_a}^2+{J'_b}^2-J'_bJ'_d+{J'_d}^2-J'_a\left(J'_b+J'_d\right)\right]\right\}^{1/2} \qquad \text{(A.2)}\\
y &= \Big[3+8{J'_a}^2+8{J'_b}^2+9J'_c-J'_b\left(9+6J'_c-4J'_d\right)+2(3J'_c-2J'_d)^2\\
&\quad -2J'_a\left(-3+7J'_b+3J'_c-2J'_d\right)-6J'_d\Big]^{1/2}\\
\chi_\pm &= \left[\cos\left(\pi x/6\right)\pm 2i\sqrt{3}\frac{\left(2J'_a-J'_b-J'_d\right)}{x}\sin\left(\pi x/6\right)\right]e^{i\pi\frac{\sqrt{3}}{6}\left(1+2J'_a+2J'_b+2J'_d\right)}\\
\lambda &= \frac{3i\left(1+2J'_b-2J'_d\right)}{x}\sin\left(\pi x/6\right)e^{i\pi\frac{\sqrt{3}}{6}\left(1+2J'_a+2J'_b+2J'_d\right)}\\
\xi &= e^{i\pi\frac{1}{\sqrt{3}}\left(2-J'_a-J'_b+2J'_d\right)}\\
\theta &= \xi e^{i\pi\sqrt{3}J'_c}\\
\tau_\pm &= \left[\cos(\frac{\pi y}{\sqrt{6}})\pm\frac{i\left(3+8J'_a-7J'_b-3J'_c+2J'_d\right)}{2\sqrt{2}y}\sin(\frac{\pi y}{\sqrt{6}})\right]e^{i\pi\frac{1}{\sqrt{3}}\left(2+J'_a+J'_b-2J'_d\right)}\\
\mu &= \frac{\sqrt{15}\left(J'_b-3J'_c+2J'_d-1\right)}{2\sqrt{2}iy}\sin(\frac{\pi y}{\sqrt{6}})e^{i\pi\frac{1}{\sqrt{3}}\left(2+J'_a+J'_b-2J'_d\right)}.
\end{aligned}
$$

In comparison, Bacon's U_1 gate has the form

$$U_1 = \begin{pmatrix} & & & \Omega & & & & & & & & \\ & & & & \Omega & & & & & & & \\ & & & & & \Omega & & & & & & \\ & & & & & & \Omega & & & & & \\ \Omega & & & & & & & & & & & \\ & & \Omega & & & & & & & & & \\ & \Omega & & & & & & & & & & \\ & & & \Omega & & & & & & & & \\ & & & & & & & \Xi & & & & \\ & & & & & & & & \Xi & & & \\ & & & & & & & & & \Gamma & \Delta & \\ & & & & & & & & & \Delta & \Theta & \\ & & & & & & & & & & & \Xi \\ & & & & & & & & & & & & \Xi \end{pmatrix} \tag{A.3}$$

where

$$\begin{aligned} \Omega &= ie^{i\frac{\pi}{2\sqrt{3}}} \\ \Xi &= e^{i\frac{2\pi}{\sqrt{3}}} \\ \Delta &= \frac{i}{2}\sqrt{\frac{5}{2}}e^{i\frac{2\pi}{\sqrt{3}}}\sin(\frac{\pi}{\sqrt{2}}) \\ \Theta &= e^{i\frac{2\pi}{\sqrt{3}}}\left[\cos(\frac{\pi}{\sqrt{2}}) + i\sqrt{\frac{3}{8}}\sin(\frac{\pi}{\sqrt{2}})\right] \\ \Gamma &= e^{i\frac{2\pi}{\sqrt{3}}}\left[\cos(\frac{\pi}{\sqrt{2}}) - i\sqrt{\frac{3}{8}}\sin(\frac{\pi}{\sqrt{2}})\right], \end{aligned}$$

and it may be verified that U_1' reduces to U_1 in the limit $J_a', J_b', J_c', J_d' \to 0$. The U_1' gate, like the U_1 gate, is applied at the beginning of the controlled-phase gate sequence and hence acts on the computational basis states. By comparing the explicit matrix representations (A.1) and (A.3) it is clear that the crucial difference between the two is the appearance of the χ_+ terms on the diagonal of U_1' (the difference between Ω and λ is irrelevant: it is equivalent to a global phase). In order for U_1' to act like U_1, i.e. in order for it not to prepare a

superposition of code states and non-code states, χ_+ must vanish. Consulting the expression (A.2) it is evident that this leads to a complicated transcendental equation relating the constants $\{J'_a, J'_b, J'_d\}$ (but not involving J'_c). A numerical solution of the condition $\chi_+ = 0$ leads to the result that the constants $\{J'_a, J'_b, J'_d\}$ can take on an infinite set of rationally related values. Upon setting the ratio J'_b/J'_d to any rational number (except 1), we may calculate a corresponding rational value of J'_a.

Bibliography

[1] D. K. Ferry, *Semiconductors* (Macmillan, New York, 1991).

[2] D. D. Awschalom and M. E. Flatté, *Nature Phys.* **3**, 153 (2007).

[3] R. Enderlein and N. J. M. Horing, *Fundamentals of Semiconductor Physics and Devices* (World Scientific, Singapore, 1997).

[4] A. Goldmann and E. E. Koch, eds., *Landolt-Börnstein Numerical Data and Functional Relationships in Science and Technology* (Springer-Verlag, Berlin, 1989).

[5] M. A. Nielsen and I. L. Chuang, *Quantum Computation and Quantum Information* (Cambridge University Press, Cambridge, U.K., 2000).

[6] A. Mizel and D. A. Lidar, *Phys. Rev. Lett.* **92**, 077903 (2004).

[7] D. Knuth, *The Art of Computer Programming* (Addison-Wesley, Reading, MA, 1981).

[8] S. Lloyd, *Science* **261**, 1569 (1993).

[9] D. P. DiVincenzo, in *Scalable Quantum Computers*, S. L. Braunstein and H.-K. Lo, eds. (Wiley-VCH, Berlin, 2001).

[10] D. Loss and P. DiVincenzo, *Phys. Rev. A* **57**, 120 (1998).

[11] A. Mizel and D. A. Lidar, *Phys. Rev. B* **70**, 115310 (2004).

[12] M. Korkusinski, I. P. Gimenez, P. Hawrylak, L. Gaudreau, S. A. Studenikin, and A. S. Sachrajda, *Phys. Rev. B* **75**, 115301 (2007).

[13] A. Yariv, *Optical Electronics in Modern Communications*, 5th ed. (Oxford University Press, Oxford, U.K., 1997).

[14] A. D. Katnani and G. Margaritondo, *J. Appl. Phys.* **54**, 2522 (1983).

[15] J. Tersoff, in *Heterojunction Band Discontinuities: Physics and Device Applications*, F. Capasso and G. Margaritondo, eds. (North-Holland, Amsterdam, 1987).

[16] G. Margaritondo and P. Perfetti, in *Heterojunction Band Discontinuities: Physics and Device Applications*, F. Capasso and G. Margaritondo, eds. (North-Holland, Amsterdam, 1987).

[17] D. Bacon, J. Kempe, D. A. Lidar, and K. B. Whaley, *Phys. Rev. Lett.* **85**, 1758 (2000).

[18] J. Kempe, D. Bacon, D. A. Lidar, and K. B. Whaley, *Phys. Rev. A* **63**, 042307 (2001).

[19] D. P. DiVincenzo, D. Bacon, J. Kempe, G. Burkard, and K. B. Whaley, *Nature* **408**, 339 (2000).

[20] D. A. Lidar and L.-A. Wu, *Phys. Rev. Lett.* **88**, 017905 (2002).

[21] D. Bacon, J. Kempe, D. P. DiVincenzo, D. A. Lidar, and K. B. Whaley, in *Proceedings of the 1st International Conference on Experimental Implementations of Quantum Computation, Sydney, Australia*, R. Clark, ed. (Rinton, Princeton, NJ, 2001).

[22] M. H. Freedman, *Commun. Math. Phys.* **234**, 129 (2003).

[23] R. Raussendorf and H. J. Briegel, *Phys. Rev. Lett.* **86**, 5188 (2001).

[24] D. A. Lidar, D. Bacon, J. Kempe, and K. B. Whaley, *Phys. Rev. A* **63**, 022307 (2001).

[25] A. M. Steane, *Nature* **399**, 124 (1999).

[26] J. Preskill, *Proc. Roy. Soc. Lond. A* **454**, 385 (1998).

[27] D. Gottesman, *Phys. Rev. A* **57**, 127 (1997).

[28] P. W. Shor, in *Proceedings of the 37th Symposium on Foundations of Computing* (IEEE Computer Society Press, Los Alamitos, CA, 1996).

[29] E. Farhi, J. Goldstone, S. Gutmann, J. Lapan, A. Lundgren, and D. Preda, *Science* **292**, 472 (2001).

[30] D. Bacon, K. R. Brown, and K. B. Whaley, *Phys. Rev. Lett.* **87**, 247902 (2001).

[31] F. R. Waugh, M. J. Berry, C. H. Crouch, C. Livermore, D. J. Mar, R. M. Westervelt, K. L. Campman, and A. C. Gossard, *Phys. Rev. B* **53**, 1413 (1996).

[32] G. Burkard, H.-A. Engel, and D. Loss, *Fortschr. Phys.* **48**, 965 (2000).

[33] X. Hu and S. Das Sarma, *Phys. Rev. A* **61**, 062301 (2000).

[34] P. Zanardi, *Phys. Rev. A* **60**, R729 (1999).

[35] L.-A. Wu and D. A. Lidar, *Phys. Rev. Lett.* **88**, 207902 (2002).

[36] L.-A. Wu, M. S. Byrd, and D. A. Lidar, *Phys. Rev. Lett.* **89**, 127901 (2002).

[37] P. Zanardi and M. Rasetti, *Phys. Rev. Lett.* **79**, 3306 (1997).

[38] D. A. Lidar, D. Bacon, J. Kempe and K. B. Whaley, *Phys. Rev. A* **61**, 052307 (2000).

[39] D. A. Lidar and K. B. Whaley, in *Irreversible Quantum Dynamics*, F. Benatti and R. Floreanini, eds. (Springer, Berlin, 2003).

[40] D. M. Bacon, Ph.D. thesis, University of California, Berkeley, 2001.

[41] M. Hsieh, J. Kempe, S. Myrgren, and K. B. Whaley, *Quant. Inf. Processing* **2**, 289 (2004).

[42] V. W. Scarola, K. Park, and S. Das Sarma, *Phys. Rev. Lett.* **93**, 120503 (2004).

[43] V. W. Scarola and S. Das Sarma, *Phys. Rev. A* **71**, 032340 (2005).

[44] W. Heitler and F. London, *Z. Physik* **44**, 455 (1927).

[45] G. Burkard, D. Loss, and D. P. DiVincenzo, *Phys. Rev. B* **59**, 2070 (1999).

[46] X. Hu and S. Das Sarma, *Phys. Rev. A* **64**, 042312 (2001).

[47] J. Levy, *Phys. Rev. Lett.* **89**, 147902 (2002).

[48] J. Levy, *Phys. Stat. Sol. B* **233**, 115322 (2003).

[49] R. de Sousa and S. Das Sarma, *Phys. Rev. B* **68**, 467 (2002).

[50] E. Yablonovitch, H. W. Jiang, H. Kosaka, H. D. Robinson, D. S. Rao, and T. Szkopek, *Proc. of the IEEE* **91**, 761 (2003).

[51] A. Barenco, C. H. Bennett, R. Cleve, D. P. DiVincenzo, N. Margolus, P. Shor, T. Sleator, J. Smolin, and H. Weinfurter, *Phys. Rev. A* **52**, 3457 (1995).

[52] E. Knill, R. Laflamme, and G. J. Milburn, *Nature* **409**, 46 (2001).

[53] D. D. Awschalom, M. E. Flatté, and N. Samarth, *Sci. Am.* **286**, 67 (2002).

[54] B. E. Kane, *Nature* **393**, 133 (1998).

[55] D. D. Awschalom and N. Samarth, *J. Mag. Mag. Mat.* **200**, 130 (1999).

[56] W. H. Lau, J. T. Olesberg, and M. E. Flatté, *Phys. Rev. B* **64**, 161301(R) (2001).

[57] J. Kainz, U. Rössler, and R. Winkler, *Phys. Rev. B* **70**, 195322 (2004).

[58] I. Žutić, J. Fabian, and S. Das Sarma, *Rev. Mod. Phys* **76**, 323 (2004).

[59] P. Seneor, A. Bernand-Mantel, and F. Petroff, *J. Phys. Cond. Mat.* **19**, 165222 (2007).

[60] S. Ghosh, W. H. Wang, F. M. Mendoza, R. C. Myers, X. Li, N. Samarth, A. C. Gossard, and D. D. Awschalom, *Nature Materials* **5**, 261 (2006).

[61] W. H. Wang, S. Ghosh, F. M. Mendoza, X. Li, D. D. Awschalom, and N. Samarth, *Phys. Rev. B* **71**, 155306 (2005).

[62] K. J. Luo, J. Y. Xu, H. Cao, Y. Ma, S. H. Chang, S. T. Ho, and G. S. Solomon, *Appl. Phys. Lett.* **77**, 2304 (2000).

[63] S. Pfalz, R. Winkler, T. Nowitzki, D. Reuter, A. D. Wieck, D. Hägele, and M. Oestreich, *Phys. Rev. B* **71**, 165305 (2005).

[64] M. I. D'yakonov and V. I. Perel', *Sov. Phys. Solid State* **13**, 3023 (1972).

[65] G. Dresselhaus, *Phys. Rev.* **100**, 580 (1955).

[66] G. L. Pearson and J. Bardeen, *Phys. Rev.* **75**, 865 (1949).

[67] H. S. W. Massey and B. L. Moiseiwitsch, *Phys. Rev.* **78**, 180 (1950).

[68] N. Sclar, *Phys. Rev.* **104**, 1559 (1956).

[69] T. C. McGill and R. Baron, *Phys. Rev B* **11**, 5208 (1975).

[70] G. D. Mahan, *Many-Particle Physics*, 3rd ed. (Plenum, New York, 2000).

[71] A. Fert, J. L. Duvail, and T. Valet, *Phys. Rev. B* **52**, 6513 (1995).

[72] G. D. Mahan, *Quantum Mechanics in a Nutshell* (Princeton University Press, Princeton, NJ, 2008).

[73] B. K. Ridley, *Quantum Processes in Semiconductors* (Clarendon Press, Oxford, U.K., 1982).

[74] S. Adachi, *GaAs and Related Materials* (World Scientific, Singapore, 1994).

[75] E. L. Ivchenko and G. E. Pikus, *Superlattices and Other Heterostructures: Symmetry and Optical Phenomena*, 2nd ed. (Springer, Berlin, 1997).

[76] M. I. D'yakonov and V. I. Perel', in *Optical Orientation*, F. Meier and B. P. Zakharchenya, eds. (North-Holland, Amsterdam, 1984).

[77] S. K. Sundaram and E. Mazur, *Nature Mat.* **1**, 217 (2002).

[78] T. Jungwirth, J. Sinova, J. Mašek, J. Kučera, and A. H. MacDonald, *Rev. Mod. Phys* **78**, 809 (2006).

[79] J. Sjakste, N. Vast, and V. Tyuterev, *Phys. Rev. Lett.* **99**, 236405 (2007).

[80] D. Taj and F. Rossi, *Phys. Rev. A* **78**, 052113 (2008).

[81] C. A. Evans, V. D. Jovanović, D. Indjin, Z. Ikonić, and P. Harrison, *IEEE J. Quant. Electron.* **42**, 859 (2006).

[82] V. Savona and W. Langbein, *Phys. Rev. B* **74**, 075311 (2006).

[83] Y. G. Semenov and K. W. Kim, *Phys. Rev. B* **75**, 195342 (2007).

[84] H. Yokoyama and S. D. Brorson, *J. Appl. Phys.* **66**, 4801 (1989).

[85] G. Björk and Y. Yamamoto, *IEEE J. Quant. Electron.* **27**, 2386 (1991).

[86] G. H. M. van Tartwijk and D. Lenstra, *Quant. Semiclass. Opt.* **7**, 87 (1995).

[87] S. L. McCall, A. F. J. Levi, R. E. Slusher, S. J. Pearton, and R. A. Logan, *Appl. Phys. Lett.* **60**, 289 (1991).

[88] B. Corbett and W. M. Kelly, *Appl. Phys. Lett.* **62**, 87 (1993).

[89] M. K. Chin, D. Y. Chu, and S.-T. Ho, *J. Appl. Phys.* **75**, 3302 (1994).

[90] F. Jahnke and S. W. Koch, *Phys. Rev. A* **52**, 1712 (1995).

[91] E. A. Viktorov and P. Mandel, *Phys. Rev. Lett.* **85**, 3157 (2000).

[92] R. S. Tucker and D. J. Pope, *IEEE J. Quant. Electron.* **19**, 1179 (1983).

[93] J. M. Kikkawa, I. P. Smorchkova, N. Samarth, and D. D. Awschalom, *Science* **277**, 1284 (1997).

[94] H. Haug and S. W. Koch, *Quantum Theory of the Optical and Electronic Properties of Semiconductors*, 5th ed. (World Scientific, Hackensack, NJ, 2009).

[95] S. Hallstein, J. D. Berger, M. Hilpert, H. C. Schneider, W. W. Rühle, F. Jahnke, S. W. Koch, H. M. Gibbs, G. Khitrova, and M. Oestreich, *Phys. Rev. B* **56**, R7076 (1997).

[96] E. Heiner and W. Kleinig, *Physica Scripta* **46**, 88 (1992).

[97] M. Bass, J. M. Enoch, E. W. von Stryland, and W. L. Wolfe, eds., *Handbook of Optics*, 2nd ed. (McGraw-Hill, New York, 1995).

[98] J. H. Davies, *The Physics of Low-Dimensional Semiconductors* (Cambridge University Press, Cambridge, U.K., 1998).

[99] W. H. Press, S. A. Teukolsky, W. T. Vettering, and B. P. Flannery, *Numerical Recipes in C*, 2nd ed. (Cambridge University Press, Cambridge, U.K., 1992).

[100] N. W. Ashcroft and N. D. Mermin, *Solid State Physics* (Harcourt, Fort Worth, TX, 1976).

[101] B. G. Streetman and S. K. Banerjee, *Solid State Electronic Devices*, 6th ed. (Pearson, Upper Saddle River, NJ, 2006).

[102] K. Gündoğdu, K. C. Hall, E. J. Koerperick, C. E. Pryor, M. E. Flatté, T. F. Boggess, O. B. Shchekin, and D. G. Deppe, *Appl. Phys. Lett.* **86**, 113111 (2005).

[103] D. Zwillinger, *Handbook of Differential Equations* (Academic Press, Boston, 1989).

[104] A. L. Garcia, *Numerical Methods for Physics*, 2nd ed. (Prentice Hall, Upper Saddle River, NJ, 2000).

[105] E. Zauderer, *Partial Differential Equations of Applied Mathematics*, 3rd ed. (Wiley-Interscience, Hoboken, NJ, 2006).

[106] W. H. Wang, Ph.D. thesis, Pennsylvania State University, 2005.

[107] G. Björk, A. Karlsson, and Y. Yamamoto, *Phys. Rev. A* **50**, 1675 (1994).

[108] J. M. Kikkawa and D. D. Awschalom, *Phys. Rev. Lett.* **80**, 4313 (1998).

[109] O. Manasreh, *Semiconductor Heterojunctions and Nanostructures* (McGraw-Hill, New York, 2005).

[110] A. F. G. Monte, S. W. da Silva, J. M. R. Cruz, P. C. Morais, A. S. Chaves, and H. M. Cox, *Phys. Lett. A* **268**, 430 (2000).

Vita

Ryan Woodworth

Education

Ph.D. in Theoretical Condensed Matter Physics, Pennsylvania State University (expected August 2009).
B.A. in Physics, Wesleyan University (May 1996).
B.A. in Mathematics, Wesleyan University (May 1996).

Awards

Homer F. Braddock Achievement Grant, Pennsylvania State University (2002-2003).
Nellie H. and Oscar L. Roberts Fellowship, Pennsylvania State University (2001-2002).
Herbert Eli Arnold Scholarship, Wesleyan University (1995).
Stanley and Sylvia Hujsak Memorial Scholarship (1992).

Publications

R. Woodworth and G. D. Mahan, "Role of diffusion in the operation of semiconductor microdisk lasers", submitted to *Journal of Applied Physics*.
G. D. Mahan and R. Woodworth, "Spin-exchange scattering in semiconductors", *Physical Review B* **78**, 075205 (2008).
R. Woodworth, A. Mizel, and D. A. Lidar, "Few-body spin couplings and their implications for universal quantum computation", *Journal of Physics: Condensed Matter* **18**, S721 (2006).
W. E. McAuliffe, R. LaBrie, R. Woodworth, C. Zhang, and R. P. Dunn, "State substance abuse treatment gaps", *American Journal on Addictions* **12**, 101 (2003).
W. E. McAuliffe, R. LaBrie, R. Woodworth, and C. Zhang, "Estimates of potential bias in telephone substance abuse surveys due to exclusion of households without telephones", *Journal of Drug Issues* **32**, 1139 (2003).
W. E. McAuliffe, R. Woodworth, C. Zhang, and R. P. Dunn, "Identifying substance abuse treatment gaps in substate areas", *Journal of Substance Abuse Treatment* **23**, 199 (2002).

Conference presentations

"Enhancement of spin lifetime in quantum well lasers using interface fluctuation quantum dots". APS March Meeting, New Orleans, LA (March 11, 2008).
"Many-body couplings in electron spin quantum computers". APS March Meeting, Los Angeles, CA (March 21, 2005).
"Many-spin interactions in quantum dot quantum computers". APS March Meeting, Montreal, Quebec, Canada (March 24, 2004).